Review: friction stir welding tools

R. Rai[1], A. De[2], H. K. D. H. Bhadeshia[3] and T. DebRoy*[1]

Friction stir welding (FSW) is a widely used solid state joining process for soft materials such as aluminium alloys because it avoids many of the common problems of fusion welding. Commercial feasibility of the FSW process for harder alloys such as steels and titanium alloys awaits the development of cost effective and durable tools which lead to structurally sound welds consistently. Material selection and design profoundly affect the performance of tools, weld quality and cost. Here we review and critically examine several important aspects of FSW tools such as tool material selection, geometry and load bearing ability, mechanisms of tool degradation and process economics.

Keywords: Friction stir welding, Tool material, Tool geometry, Load bearing ability

Introduction

A friction stir welding (FSW)[1–5] tool is obviously a critical component to the success of the process. The tool typically consists of a rotating round shoulder and a threaded cylindrical pin that heats the workpiece, mostly by friction, and moves the softened alloy around it to form the joint. Since there is no bulk melting of the workpiece, the common problems of fusion welding such as the solidification and liquation cracking, porosity and the loss of volatile alloying elements are avoided in FSW. These advantages are the main reasons for its widespread commercial success for the welding of aluminium and other soft alloys. However, the FSW tool is subjected to severe stress and high temperatures particularly for the welding of hard alloys such as steels and titanium alloys and the commercial application of FSW to these alloys is now limited by the high cost and short life of FSW tools.[4,6,7]

Although significant efforts have been made in the recent past to develop cost effective and reusable tools, most of the efforts have been empirical in nature and further work is needed for improvement in tool design to advance the practice of FSW to hard alloys. This paper critically reviews recent work on several important aspects of FSW tools such as the tool geometry, issues of material selection, microstructure, load bearing ability, failure mechanisms and process economics.

Commonly used tool materials

Tool steel

Materials such as aluminium or magnesium alloys, and aluminium matrix composites (AMCs) are commonly welded using steel tools.[8–17] Steel tools have also been used for the joining of dissimilar materials in both lap and butt configurations.[18–25] Lee *et al.*[18] welded Al–Mg alloy with low carbon steel in lap joint configuration using tool steel as tool material without its excessive wear by placing the softer Al–Mg alloy on top of the steel plate and avoiding direct contact of the tool with the steel plate. In butt joint configuration, the harder workpiece is often placed on the advancing side and the tool is slightly offset from the butt interface towards the softer workpiece.[20–23] Cold worked X155CrMoV12-1 tool steel was used by Meran and Kovan[25] for welding of 99·5% pure Cu with CuZn30 brass in butt joint configuration. Oil hardened (62 HRC) steel tool has been used to successfully weld Al 6061 + 20 vol.-%Al_2O_3 AMC[9] and Al 359 + 20 vol.-%SiC AMC.[11] Tool wear during welding of metal matrix composites is greater when compared with welding of soft alloys due to the presence of hard, abrasive phases in the composites. For FSW of AMCs, some studies[9,11,26] have shown that the tool wears initially and obtains a self-optimised shape after which wear becomes much less pronounced. This self-optimised final shape, which depends on the process parameters and is generally smooth with no threads, can reduce wear when used as the initial tool shape. Total wear was found to increase with rotational speed and decrease at lower traverse speed, which suggests that process parameters can be adjusted to increase tool life.[9,11] Prado *et al.*[9] argued against the need for threads in the tools because the tools continued to produce good quality welds even after the threading had worn out and tool had obtained a smooth shape.

Polycrystalline cubic boron nitride (pcBN) tools

Owing to high strength and hardness at elevated temperatures along with high temperature stability, pcBN is a preferred tool material for FSW of hard alloys such as steels and Ti alloys.[27–36] Furthermore, the low coefficient of friction for pcBN results in smooth weld surface.[37] However, due to high temperatures and pressures required in the manufacturing of pcBN, the tool costs are very high. Owing to its low fracture

[1]Department of Materials Science and Metallurgy, Pennsylvania State University, University Park, PA 16802, USA
[2]Department of Mechanical Engineering, Indian Institute of Technology, Bombay, Mumbai 400076, India
[3]Department of Materials Science and Metallurgy, University of Cambridge, Pembroke Street, Cambridge CB2 3QZ, UK

*Corresponding author, email debroy@psu.edu

Published by Maney on behalf of the Institute
Received 18 January 2011; accepted 3 February 2011
DOI 10.1179/1362171811Y.0000000023

toughness, pcBN also has a tendency to fail during the initial plunge stage. Maximum weld depths with pcBN tools are currently limited to 10 mm for welding of steels and Ti alloys.[37]

Boron nitride has two crystal structures, the hexagonal and cubic varieties. The hexagonal form has a layered structure and hence is more suited as a lubricant. The cubic (zinc blende structure) form is usually prepared by subjecting the hexagonal version to high temperatures and pressures, similar to what is followed in producing diamond from graphite. The cubic form is second in hardness only to diamond and has greater thermal and chemical stability than carbon. The phase is also chemically inert to iron,[38] reportedly even up to 1573 K.[39,40] Like diamond, pcBN has a high thermal conductivity which helps avoid the development of hot spots on tools. A high thermal conductivity also helps in the design of liquid cooled tools.[41] The best properties are obtained with single phase cubic boron nitride (cBN), produced without using any binder. Such a material can be prepared by sintering commercially pure hexagonal boron nitride at high pressures (6–8 GPa) and temperatures (1773–2673 K).[39,42,43] The fracture toughness for pcBN with a grain size in the range 2–12 μm is found to be $\sim$7 MPa $m^{1/2}$ at ambient temperature.[42] Mixtures of cBN with binders exhibit a ductile to brittle transition temperature in the range 1323–1423 K depending on the fraction of the nitride relative to the other phases.[44]

Research on the wear properties of pcBN as a cutting tool material for hardened steels and superalloys has shown that abrasion and diffusion are the wear mechanisms.[45] Konig and Neises[45] studied the wear of two grades of pcBN with different sizes of the cBN and binder. The binder was AlN–AlB_2 in one grade and TiC based binder with some AlB_2 and W in the other grade. The cBN contents were $\sim$88 and 50% in the first and second grades respectively. Since the binder is typically much softer than the ceramic, its concentration affects the wear resistance of the tool. Heating of a tool at 1223 K showed that the binder was recrystallised whereas the cBN crystals remained unchanged.[45] No evidence of chemical reaction between the binder and the workpiece material (100Cr6 steel) was found. The weakening of the binder due to structural changes was assumed to reduce the wear resistance of pcBN tools. Konig and Neises[45] evaluated pcBN grades of FSW tools based on real cutting tests and model tests. In model tests, diffusion couples of pcBN and 100Cr6 were exposed to 1223 K for 20 h followed by abrasion of pcBN surfaces with a diamond indenter. Since the relative wear of the two grades of pcBN in cutting tests was opposite to that observed in the model tests, they argued for possible presence of other wear mechanisms. They suggested that the breaking out of cBN crystals following removal of binder, and conversion of cBN to its soft, hexagonal form at high temperatures could be the possible wear mechanisms. Hooper *et al.*[46] compared the wear in TiC–cBN tool with that in cBN and discussed a different wear mechanism. The chemical wear of cBN is exacerbated by the formation of extensive defect structures above a threshold temperature of 1200 K. They suggested that the lower thermal conductivity of TiC–cBN based tool compared with the cBN based tool resulted in higher temperatures and a more stable protective layer. Several other studies[47–49] have been carried out on the mechanisms of cutting tool wear. However, it is not clear if, and to what extent, these various wear mechanisms are relevant to the FSW process.

Tool wear affects not only the tool life but also the weld characteristics. Park *et al.*[34] examined FSW of ferritic, duplex and austenitic steels with pcBN tool and found that boron and nitrogen pick-up from worn tool was more for steels having higher steady state flow stress. Nitrogen contents in the stir zones of both ferritic and duplex steels, as well as in the retreating side of the austenitic steel, were about the same as that in the base metal. On the other hand, the nitrogen content in the advancing side of austenitic steel varied between two to five times the base metal content. Boron from the pcBN tool reacted with chromium in austenitic steels to form borides leaving the weld material susceptible to corrosion and pitting. Zhang *et al.*[30] used pcBN tool to weld commercially pure Ti and observed severe tool wear. The debris from the tool reacted with Ti to form TiB_2; both TiB_2 and pcBN debris contributed to the grain refinement as well as increase in surface hardness.

Nelson[50] reported a pcBN tool life sufficient for the welding of a 45 m long high strength low alloy steel; although the thickness of the steel was not reported, a clue can be obtained from later work where high strength low alloy-65 of 6 mm thickness was welded using pcBN tools.[51] Sorensen[52] investigated the wear and fracture sensitivity of three grades of pcBN tools and obtained a tool life of $\sim$60 m for the welding of a structural steel; although the thickness of the steel was not stated, it is known that the maximum weld depth achievable now for pcBN tools is 10 mm.[37] In an FSW study done by Jasthi *et al.*[53] on Fe–Ni alloy (invar), higher thermal conductivity of pcBN (100–250 W m^{-1} K^{-1}) compared with that of the tungsten–rhenium alloy, W–25 wt-%Re (55–65 W m^{-1} K^{-1}) resulted in higher heat loss and lower workpiece temperatures. The traverse and vertical direction forces on the tool pin were much higher for pcBN than for W–25 wt-%Re tool; the lower forces in case of W–25 wt-%Re tool were attributed to the higher workpiece temperatures. Tool wear in pcBN was insignificant compared with W–Re and tool debris was found in the workpiece in the latter case. The coefficient of thermal expansion and ultimate strengths of the welds were similar to those of the base metal for both the tools. Microstructural differences, such as the presence of recrystallised grains in welds made with pcBN tool, were attributed to differences in thermal conductivities of the two tool materials.

W based tools

Commercially pure tungsten (cp-W) is strong at elevated temperatures but has poor toughness at ambient temperature, and wears rapidly when used as a tool material for FSW of steels and titanium alloys. It is known that exposure of cp-W to temperatures in excess of 1473 K causes it to recrystallise and embrittle on cooling to ambient temperature. Addition of rhenium reduces the ductile to brittle transition temperature by influencing the Peierls stress for dislocation motion.[54] This led to the development of tungsten–rhenium alloys, with W–25 wt-%Re as a candidate material for FSW tools,[55] and more recently, a variant of this reinforced

with ~2% of HfC.[56] Steels and titanium alloys are successfully welded by W–25 wt-%Re tool. For example, Weinberger *et al.*[57] produced good quality welds on martensitic precipitation hardened steels using a W–25 wt-%Re alloy tool, which is about four times stronger than cp-W at 1273 K.[58] It has at the same time a lower ductile to brittle transition temperature than cp-W and improved fracture resistance and wear resistance at room temperature.[37] Liyanage *et al.*[59] used W–25 wt-%Re alloy tool to make dissimilar welds between Al alloy and steel, and between Mg alloy and steel with some tool wear. Gan *et al.*[58] modelled the degradation of cp-W tool through plastic deformation in the welding of L80 steel. Considering only plastic deformation they recommended a minimum yield strength at an elevated temperature (1273 K) for their welding conditions which W–25 wt-%Re alloy and pcBN could satisfy. Since pcBN is brittle and boron from pcBN may get dissolved into base material to form an undesirable phase, the W–25 wt-%Re alloy was recommended by the authors. Their work did not consider the influence of bending and torsion loads on tool, or erosion of tool material. It should be noted that Re is an incredibly expensive element, and the processing required is also costly.[60] As a consequence, such tools are unlikely to see widespread exploitation, in spite of their elevated temperature capabilities and reasonable ductility.

Tungsten carbide (WC) based tools have also been exploited in investigations of the feasibility of FSW of steel[61] and titanium alloys.[62,63] The toughness of WC is said to be excellent and the hardness is ~1650 HV. The material is apparently also insensitive to sudden changes in temperature and load during welding trials.[61] Given the often proprietary nature of tool data, there is little information available on the chemical inertness of the material with respect to the metal being joined. Composite tools with different combinations of pin and shoulder materials were tried by Reshad Seighalani *et al.*[62] They found that a tool with a W shoulder and WC pin at a 1° tilt angle resulted in defect free welds with yield and tensile strengths similar to those of the base metal. Teimournezhad and Masoumi[64] used a tool with a non-threaded WC pin and a high speed steel shoulder to investigate the formation of onion rings in FSW of 4 mm thick Cu plates. Reynolds *et al.*[65,66] welded 304L stainless steel and DH 36 carbon steel with a W alloy tool (composition not reported) and were able to obtain weld tensile properties very similar to or better than that for the base metal.

Choi *et al.*[67] used WC–13 wt-%Co and WC–13 wt-%Co–6 wt-%Ni–1·5 wt-%Cr_3C_2 tools to friction stir spot weld low carbon steel plates. Based on X-ray diffraction and scanning electron microscopy analysis, they proposed three potential mechanisms of tool wear. First, the oxidation of WC at high temperatures may result in carbon monoxide (CO) gas at a pressure greater than the strength of the material. However, it is not clear how the oxygen was available to the immersed tool. Second, the Co binder may transform from ductile face centred cubic to brittle hexagonal close packed at high temperature resulting in fracture of the binder and its removal from the tool. Third, the possible formation of ternary W–Fe–O compounds on the tool surface may degrade the tool. It was suggested that the addition of CrC_2 to WC–Co reduced the tool wear by reducing oxidation of WC. A WC–Co alloy tool with threaded pin has been used to weld AMCs with 30 vol.-% of SiC particulates.[68] The shoulder wear and longitudinal pin wear were found to be smaller than the radial wear of pin. The radial pin wear started near the shoulder and progressed further along the length of the pin with increasing travel distance. Wear rate in mm per unit travel distance was found to be higher for low welding speeds and was attributed to the greater time available for the wear phenomenon to occur. The rate of wear was the highest at the start of the welding and was found to decrease with increasing usage. This observation is in line with other studies[9,26,69] with cylindrical pins where it has been found that the tool pins have suffered severe deformation initially and obtained a self-optimised shape after which wear rate has decreased significantly.

Other tungsten based alloys have also been used for the welding of both low and high melting point alloys. For example, Edwards and Ramulu[70] used a W–La alloy (composition not reported) tool to study FSW of Ti–6Al–4V alloy. Tools made of a tungsten alloy Densimet (composition not reported) were used by Yadava *et al.*[71] to weld AA 6111-T4 aluminium alloy.

Other tools

High hardness, low coefficient of thermal expansion and high thermal conductivity of Si_3N_4 make it a useful cutting tool material.[72] Coating with an inert material such as diamond or TiC can result in further improvements in its high temperature wear resistance.[72,73] Even though the property requirements for cutting and FSW tools are similar, use of Si_3N_4 tools in FSW is not very common. Ohashi *et al.*[73] studied the welding of DP 590 steel with Si_3N_4 tools and found that O and N contamination resulted in the formation of finer martensite. The contamination of workpiece by Si and N from the tool was prevented by TiC/TiN coating. Sintered TiC welding tool, with a water cooling arrangement to extract excessive heat from the tool, has been used for successful FSW of titanium.[74] Molybdenum based alloy tool has been used to weld AISI 1018 mild steel[75] and Ti–15V–3Cr–3Al–3Sn alloy.[76]

Tables 1–6 list the tool materials, tool geometries and welding variables used to weld some of the common engineering materials.

Tool material selection

Weld quality and tool wear are two important considerations in the selection of tool material, the properties of which may affect the weld quality by influencing heat generation and dissipation. The weld microstructure may also be affected as a result of interaction with eroded tool material. Apart from the potentially undesirable effects on the weld microstructure, significant tool wear increases the processing cost of FSW. Owing to the severe heating of the tool during FSW, significant wear may result if the tool material has low yield strength at high temperatures. Stresses experienced by the tool are dependent on the strength of the workpiece at high temperatures common under the FSW conditions. Temperatures in the workpiece depend on the material properties of tool, such as thermal conductivity, for a given workpiece and processing parameters. The coefficient of thermal expansion may affect the thermal stresses in the tool. Other factors that may

Table 1 Tool materials, geometries and welding variables used for FSW of several magnesium alloys*

Workpiece material	Tool material	Tool shape and size	Operating parameters	Remarks	Reference
AZ31 Mg, 1·5 mm thick	H13 steel	SD: 10 mm; PD: 4 mm; PL: 1·8 mm; PS: SCT, 3F with M4 threads	1000–3000 rev min^{-1}; dwell time: 1, 4 s; plunge rate: 0–10 mm s^{-1}; FSSW		79
AZ31 Mg, 1·5 mm	H13 steel, 46–48 HRC	SD: 10 mm; PD: 4 mm; PL: 1·8 mm; PS: SCT, and threaded and unthreaded 3F	1000–3000 rev min^{-1}; dwell time: 1 s; plunge rate: 2·5 mm s^{-1}; FSSW	Welds with 3F/threaded superior to those with SCT	115
AZ31B-H24 Mg alloy, 2 mm		PD: 3·175 mm; PL: 1·65 mm; PS: SC, LHT, RHT	1000–2000 rev min^{-1}; 300–1800 mm min^{-1}	Joint efficiencies: 74–83%	101
AZ31B Mg alloy, 6 mm	Mild steel, stainless steel, armour steel, high carbon steel, high speed steel	SD: 15, 18, 21 mm; PS: SC, TC, SCT, triangular and square; PL: 5·7 mm; PD: 6 mm	1600 rev min^{-1}; 40 mm min^{-1}; 0° tilt	Joint efficiencies: 48·8–96·7%	134
AZ31B-H24 Mg alloy, 2 mm	H13 steel	SD: 19 mm; PL: 2–3·5 mm; PD: 6·35 mm	1200 mm min^{-1}; 500–2000 rev min^{-1}	Joint efficiencies: up to 62%	135

*SD: shoulder diameter; PD: pin diameter; PL: pin length; PS: pin shape; SC: straight circular; TC: tapered circular; SCT: straight circular threaded; LHT (RHT): left (right) handed thread; 3F: three flats; FSSW: friction stir spot welding. Joint efficiency is the ratio of the tensile strength of the joint to that of the base metal.

Table 2 Tool materials, geometries and welding variables used for FSW of several aluminium alloys*

Workpiece material	Tool material	Tool shape and size	Operating parameters	Remarks	Reference
6111-T4 Al alloy, 0·9 mm thick	H13 steel	SS: flat with scroll; SD: 10 mm; PL: 0–1·6 mm	2000 rev min^{-1}; dwell time: 2·5 s; plunge rate: 2·5 mm s^{-1}; FSSW	Better quality with pinless tool	136
7075-T7351, 6·35 mm		PS: Triflute, Trivex	394 and 457 rev min^{-1}; 300–540 mm min^{-1}	Weld UTS: 470–488 MPa	133
7075-T7351; 6·35 mm, 16 mm	1. MP159; 2. Dievar tool steel; 3. MP159 pin, H13 shoulder	PS: threaded	190–457 rev min^{-1}; 0·3–1·4 mm rev^{-1}	Surface scaling and voiding problems	137
Al alloys, 5 mm		SS: concave; SD: 15 mm; PS: SC, SCT, triangular; PL: 4·7 mm, 6 mm	600–1500 rev min^{-1}; 25–1000 mm min^{-1}; 3° tilt	Peak joint efficiencies: 70–100%	82
7020-T6 Al alloy, 4 mm	Steel	SD: 10–20 mm, flat; PD: 3–8 mm; PL: 4·2 mm; PS: frustum and SC	1400 rev min^{-1}; 80 mm min^{-1}	Peak joint efficiency: 92%	80
6082-T6 Al, 1·5 mm		SS: scroll, cavity, fillet; PD: 1·7 mm; PS: SC; PL: 1·2 mm	1810 rev min^{-1}; 460 mm min^{-1}; 2° tilt	Joint efficiencies: ~76%	138
6061-T6 Al, 9·5 mm and 12·7 mm	H13 steel	SD: 25·4 mm; PD: 5·2–7·6 mm; PL: 1·8–7·1 mm	650 rev min^{-1}; 150 or 200 mm min^{-1}; 3° tilt		120
6061-T6 Al, 6·3 mm		SS: concave; SD: 26 mm; PD: 5·6 mm; PL: 5·9 mm; PS: SCT	286–1150 rev min^{-1}; 30–210 mm min^{-1}		118
5754 Al, 1·32 mm	H13 steel	SS: concave, convex, flat; SD: 12 mm; PD: 5 mm; PL: 1·6 mm	1500 rev min^{-1}; dwell time: 2 s; plunge rate: 20 mm min^{-1}; FSSW		116
A319 and A413 Al alloy, 6 mm	Tool steel	PD: 6 mm	1000 rev min^{-1}; 120 mm min^{-1}	No property degradation in weld metal	13
7020-T6 Al, 4 mm	High carbon steel	SS: concave; SD: 13 mm; PS: SC, TC3F; PL: 3·19 mm: PD: 5 mm	300–1620 rev min^{-1}; 100–900 mm min^{-1}; 2·5° tilt		77

*SD: shoulder diameter; PL: pin length; PD: pin diameter; PS: pin shape; SS: shoulder shape; SC: straight circular; SCT: straight circular threaded; TC3F: tapered circular with three flats; UTS: ultimate tensile strength; FSSW: friction stir spot welding. Joint efficiency is the ratio of the tensile strength of the joint to that of the base metal.

Table 3 Tool materials, geometries and welding variables used for FSW of several metal matrix composites*

Workpiece material	Tool material	Tool shape and size	Operating parameters	Remarks	Reference
6061-T6 Al+ 20%Al_2O_3, 5 and 6 mm thick	AISI oil hardened Tool steel (62 HRC)	SD: 19 mm; PS: SCT; PD: 6·3 mm	500–2000 rev min^{-1}; 60–540 mm min^{-1}; 1° tilt	No wear after some distance (150–300 mm) depending on process parameters	9, 10
Al 359+ 20%SiC, 4 mm	AISI oil hardened tool steel (62 HRC)	SD: 19 mm; PS: SCT; PD: 6·3 mm; PL: 3·6 mm	500–1000 rev min^{-1}; 360 and 660 mm min^{-1}		11
Al 359+ 20 vol.-%SiC, 4 mm	AISI oil hardened steel	SD: 19 mm diameter; PD: 6·3 mm	1000 rev min^{-1}; 60–540 mm min^{-1}		26
Al–10 wt-%TiB_2, 6 mm	High C high Cr steel (60–62 HRC)	SD: 16 mm; PS: SSq, TSq, SOct, TOct, SHex, THex,	2000 rev min^{-1}; 30 mm min^{-1}	Joint efficiencies: 78·9–99·5%	84
Al–15 wt-% Mg_2Si, 6 mm	H13 steel	SD: 18 mm; PS: TCT; PL: 5·7 mm	710–1400 rev min^{-1}; 125 mm min^{-1}	Joint efficiencies: 80–98%	14
AA 6061–(3–7)%TiC, 6 mm	High C, high Cr steel	PS: SSq, TSq, SHex, THex, TOct	30–135 mm min^{-1}	Joint efficiencies: 72–114%	139

*SD: shoulder diameter; PL: pin length; PD: pin diameter; PS: pin shape; SCT: straight circular threaded; TCT: tapered circular threaded; SSq: square; TSq: tapered square; SHex: hexagonal; THex: tapered hexagonal; TOct: tapered octagonal. Joint efficiency is the ratio of the tensile strength of the joint to that of the base metal.

Table 4 Tool materials, geometries and welding variables used for FSW of several titanium and its alloys*

Workpiece material	Tool material	Tool shape and size	Operating parameters	Remarks	Reference
cp-Ti, 3 mm	pcBN	SS: concave; SD: 15 mm; PS: tapered at 45° and truncated; PL: 1·7 mm; PD_t: 5·1 mm	200 rev min^{-1}; 50 mm min^{-1}; Ar shield	Severe tool wear	30
Ti, 3 mm	1. HSS; 2. WC pin, HSS shoulder; 3. WC pin, W shoulder	SD: 18 mm; PS: SC; PD: 5 mm; PL: 2·85 mm	(1250 rev min^{-1}; 32 mm s^{-1}), (1500 rev min^{-1}; 60 mm min^{-1}); tilt angle: 1, 3°	Up to 100% joint efficiency obtained with W–WC tool with low wear; low strength and high wear with other tools	62
Ti–6Al–4V, 3–12 mm	W–La alloy	SD: 19–32 mm; PS: tapered; PL: 2·8–13·3 mm	150–750 rev min^{-1}; 50–200 mm min^{-1}	Joint efficiency: >100%	70, 140–142
Ti, 2 mm	WC–Co	SD: 15 mm; PL: 2 mm; PD: 6 mm	200–350 rev min^{-1}; 50–150 mm min^{-1}	Joints that failed in BM for some cases	143
Timetal 21S, 1·59 mm	W alloy	Proprietary	200 rev min^{-1}; 51–305 mm min^{-1}; Ar shield	No volumetric defects found	144
Ti, 5·6 mm	Sintered TiC		1000 rev min^{-1}; 500 mm min^{-1}	Joint efficiency: 97%	74
Ti–6Al–4V, 2 mm	W–3 wt-%Re	SD: 11 mm; PL: 1·8 mm; PD_t: 6 mm; PD_b: 4 mm	400 rev min^{-1}; 50 mm min^{-1}; 2·5° tilt; Ar shield	No volumetric defects found	145
Ti-5111 plate, 12·7 mm	W alloy	PL: 12·7 mm; PD_t: 25·4 mm; PD_b: 9·5 mm	140 rev min^{-1}; 51 mm min^{-1}		146
Ti–15V–3Cr–3Al–3Sn, 3 mm	Mo based alloy	SS: convex; SD: 15 mm; PD_t: 5·1 mm; PD_b: 3 mm	400 rev min^{-1}; 60 mm min^{-1}; Ar shield		76

*SD: shoulder diameter; PD: pin diameter; PL: pin length; PD_t: pin diameter at the top (larger diameter) for tapered pin; PD_b: pin diameter at the bottom (smaller diameter) for tapered pin; PS: pin shape; SS: shoulder shape; SC: straight circular; BM: base metal. Joint efficiency is the ratio of the tensile strength of the joint to that of the base metal.

Table 5 Tool materials, geometries and welding variables used for FSW of several ferrous alloys*

Workpiece material	Tool material	Tool shape and size	Operating parameters	Remarks	Reference
Fe–1·02C–0·24Si–0·37Mn–1·42Cr, 2·3 mm thick	pcBN	SD: 14 mm; PL: 2 mm; PD_t: 5·8 mm; PD_b: 4 mm	400–800 rev min^{-1}; 76 mm min^{-1}; Ar	Defect free welds produced at all rates	31
NSSC 270 superaustenitic SS, 6 mm	pcBN	Convex scrolled shoulder step spiral (CS4) pin tool	400 and 800 rev min^{-1}; 30–60 mm min^{-1}	Strength and ductility comparable with that of the base metal at 400 rev min^{-1}; more intermetallic phases at 800 rev min^{-1} caused poor joints	36
SAF 2507 super duplex SS, 4 mm	pcBN	SD: 25 mm; PL: 3·8 mm	450 rev min^{-1}; 60 mm min^{-1}; 3·5° tilt	Joint strength similar to base metal	32
DP 780 carbon steel, 1·5 mm	pcBN	SS: concave; PS: tapered, various step geometries; PL: 2 mm	800–1600 rev min^{-1}; dwell time: 1–10 s; FSSW	Lap shear strengths greater than RSW achieved for dwell time 8 s or greater	33
430 ferritic, 329J4L duplex, 304, 316L and 310 steels, 6 mm	pcBN	PL: 4·29 mm	550 rev min^{-1}; 80 mm min^{-1}; 3·5° tilt angle; Ar	Significant tool wear	34
Hot stamped boron steel, 1·4 mm	pcBN	SS: concave; SD: 10·2 mm; PL: 2·3 mm; TC3F	35 mm overlap welds; 800–2000 rev min^{-1}; 1·9–10·5 s welding time	'Hundreds' of welds made without significant wear	35
304L SS, 3·2 mm	W alloy	SD: 19 mm	300 and 500 rev min^{-1}; 102 mm s^{-1}; Ar	UTS of weld lager than UTS of base metal	65
15-5PH, 2·6 mm	W–25%Re	SS: concave; SD: 16 mm; PD: 6 mm; PL: 2·1 mm	300–450 rev min^{-1}; 60–350 mm min^{-1}; tilt angle: 3°; Ar	Joint efficiencies: 80–98%; tool wear at pin tip and shoulder edge	57
DP 600, 1·22 mm	W–25%Re	SD: 10 mm; PS: TC; PL: 1·7 mm; PD: 4–5·1 mm	3000 rev min^{-1}; plunge rate: 30–60 mm min^{-1} (FSSW)	Properties similar to RSW	55
Low carbon steel, 0·6 mm	1. WC–13% Co; 2. WC–13%Co+6%Ni, 1·5%Cr_3C_2	PS: SC	1600 rev min^{-1}; plunge rate: 15 mm min^{-1} (FSSW)	Acceptable strengths for all 500 welds; self-optimised tool after high initial wear	67
Carbon steel, 1·6 mm	WC based	SD: 12 mm; PD: 4 mm; PS: SC; PL: 1·4–1·5 mm	100–800 rev min^{-1}; 25–400 mm min^{-1}; 3° tilt	Joints stronger and more ductile than base metal	147, 148
SK5 steel, 1·6 mm	WC based	SD: 12 mm; PD: 4 mm; PL: 1·5 mm	100–400 rev min^{-1}; 100–200 mm min^{-1}; 3° tilt; Ar shield	Joints strengths similar to or higher than base metal	149
AISI 1018 mild steel, 6·3 mm	Mo and W based tools		25·4–102 mm min^{-1}	Defect free welds were obtained and failure occurred in base metal; greatest tool wear occurred during plunge stage	75
DP 590 steel, 1·2 mm	Si_3N_4, with and without TiC, TiN coating	SS: concave; SD: 10 mm; PL: 1·3 mm; PD: 4 mm	3000 rev min^{-1}; Ar (FSSW lap joint)	Contaminations with Si and N from tool caused reduction in strength	73

*SD: shoulder diameter; PD: pin diameter; PL: pin length; PD_t: pin diameter at the top (larger diameter) for tapered pin; PD_b: pin diameter at the bottom (smaller diameter) for tapered pin; PS: pin shape; SS: shoulder shape; SC: straight circular; TC: tapered circular; FSSW: friction stir spot welding; RSW: resistance spot welding; UTS: ultimate tensile strength.

influence tool material selection are hardness, ductility and reactivity with the workpiece material. The tool hardness is important in mitigating surface erosion due to interaction with particulate matter in the workpiece. The brittle nature of ceramics such as pcBN may be undesirable if there is a significant probability of breakage due to vibrations or accidental spikes in loads. Tool degradation may be exaggerated if the tool material and workpiece react to form undesirable phases.

The properties of some of the commonly used tool materials are given in Table 7 along with remarks regarding their suitability for welding specific materials. Because of their high temperature strength, pcBN and W based alloys are commonly used tool materials for FSW of harder alloys. Good quality welds have been obtained for welding of steels for both tool materials. W–25 wt-%Re alloy tool, the most common W based tool material, undergoes significant wear compared with the pcBN tool which has superior wear resistance and abrasive properties. The thermal conductivity of the tool material determines the rate of heat removal and affects the temperature fields, flow stresses and weld

Table 6 Tool materials, geometries and welding variables used for FSW of several dissimilar materials*

Workpiece material	Tool material	Tool shape and size	Operating parameters	Remarks	Reference
Fe with Ni, 6·25 mm thick	pcBN		Butt welds		150
AA 6061-T651 AA, 6 mm with SS 400 steel, 6 mm	AISI 4140	PS: SC; PD: 6–8 mm	Butt welds; 550–800 rev min^{-1}; 54–90 mm min^{-1}		21
Ductile iron with low carbon steel, 3 mm	WC–Mo	SD: 12 mm; PS: SC; PD: 3·6 mm; PL: 2·8 mm	Butt welds; 982 rev min^{-1}; 72 mm min^{-1}	Defect free welds; higher strength after heat treatment	151
2024-T3 Al alloy with Ti–6Al–4V, 2 mm	Tool steel	SS: concave; SD: 18 mm; PS: threaded and tapered; PD: 6 mm	800 rev min^{-1}; 80 mm min^{-1}	UTS of joint 73% of that for the Al alloy	23
AZ31 Mg alloy, 1·6 mm and low carbon steel, 0·8 mm	SKD61 tool steel	SD: 15 mm; PL: 1·5, 1·8 mm; PD: 5 mm	Lap welds; 240 rev min^{-1}; 100–300 mm min^{-1}; 3° tilt	Joint strength was greatly affected by welding speed and pin length	152, 153
AZ31 Mg alloy, 1·3 mm with AA 5083, 1·2 mm		SD: 10 mm; PD: 4 mm; PL: 1·6 mm	FSSW lap welds; 1500–2250 rev min^{-1}; dwell time: 2–5 s	Defect free welds with thick layer of brittle intermetallics	154
Ti with 304L SS, 4 mm	WC	SD: 28 mm; PL: 2·5 mm; PD: 8 mm	560–1100 rev min^{-1}; 25–80 mm min^{-1}; 2° tilt	Maximum failure load was 73% of that for cp-Ti	155
ADC 12 Al, 4 mm, with Ti, 2 mm	WC–Co	SD: 15 mm; PL: 3·9 mm; PD: 5 mm	Lap weld, 1500 rev min^{-1} 60–120 mm min^{-1}; 3° tilt	Maximum failure load was 62% of that for the Al alloy	63
AA 1050, 2·5 mm with 22MnB5 steel, 1·8 mm	WC–Co with AlCrN coating	Concave shoulder; SD: 12 mm; PS: TC; PD_b: 2 mm; PL: 2·7 mm	FSSW lap welds; 1000–2000 rev min^{-1}; dwell time: 2 s	30 μm wear of tool tip after 32 welds	156
AA 6061-T6, 1·5 mm, with Cu, 1·5 mm	H13 tool steel	SD: 10 mm; PD: 4 mm; PL: 1·83, 2·60 mm	FSSW lap welds; 1000–3000 rev min^{-1}; dwell time: 3, 6 s; plunge depth: 0, 0·13 mm	Joint strength greatly influenced by pin length and rate	157
AZ31B, AZ61A and AZ91D, with Ti plate, 2 mm	SKD61 tool steel	SD: 15 mm; PL: 1·9 mm; PD: 5 mm	Ti on the retreating side; 850 rev min^{-1}; 50 mm min^{-1}; 3° tilt	UTS of weld was lower for higher Al content in the Mg–Al–Zn alloy	158

*SD: shoulder diameter; PD: pin diameter; PL: pin length; PD_b: pin diameter at the bottom (smaller diameter) for tapered pin; PS: pin shape; SC: straight circular; TC: tapered circular; UTS: ultimate tensile strength; FSSW: friction stir spot welding.

microstructure. High thermal conductivity of pcBN avoids the formation of hot spots on tools and helps in the design of liquid cooled tools.[41] However, a high thermal conductivity may be undesirable if excessive removal of heat from the tool/workpiece interface requires very high tool rotational speeds to adequately soften the workpiece and to reduce tool stresses. The appropriate value of thermal conductivity depends on the process variables, workpiece material and other tool material properties.

Tool erosion under FSW conditions is often worsened by reactions of the tool with the workpiece or oxygen in the atmosphere. Oxidation of the tool may occur both during the plunge stage and after a welding operation when the hot tool is exposed to the environment. Metals such as chromium and titanium form a tenacious and coherent oxide layer that protects the surface from further oxidation. On the other hand, WO_3 that forms on tungsten vaporises as a gas, leaving the surface unprotected. If the oxide layer is not tenacious enough and breaks down under the severe thermomechanical conditions in FSW, the reactivity of the tool will be an important consideration in the selection of tool material. The tendency of a pure metal to react with oxygen is given by the standard Gibbs energy of oxidation for 1 mole of oxygen. Figure 1 shows the Ellingham diagram for some of the metals used for FSW tools. Metals higher up in the figure are less likely to oxidise compared with those below them. The high hardness, low reactivity with oxygen and high temperature strength of metals such as tungsten, molybdenum and iridium make them good choices as tool materials. These tool properties can be enhanced further by the addition of alloying elements or coating the tool with a hard, wear resistant material.

Tool geometry

Tool geometry affects the heat generation rate, traverse force, torque and the thermomechanical environment experienced by the tool. The flow of plasticised material in the workpiece is affected by the tool geometry as well as the linear and rotational motion of the tool. Important factors are shoulder diameter, shoulder surface angle, pin geometry including its shape and size,

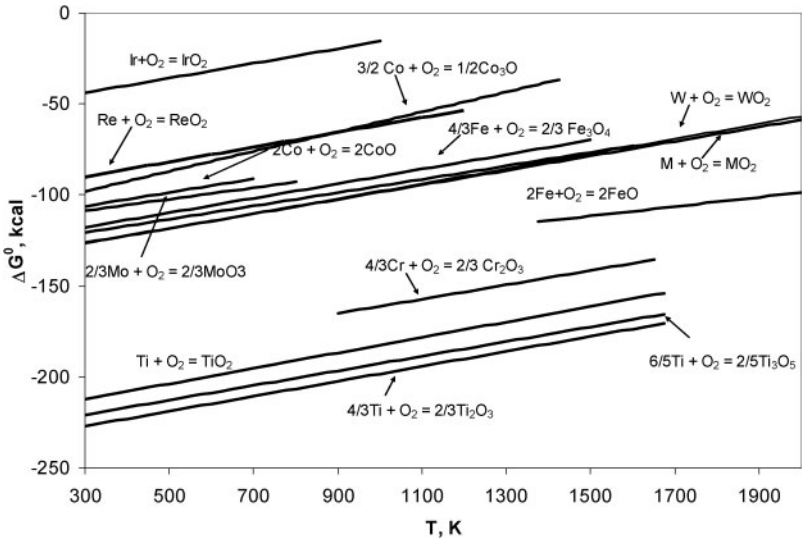

1 Ellingham diagram for some of metals used in FSW tools[132]

and the nature of tool surfaces.[8,77–88] These features are discussed here.

Shoulder diameter

The diameter of the tool shoulder is important because the shoulder generates most of the heat, and its grip on the plasticised materials largely establishes the material flow field. Both sliding and sticking generate heat whereas material flow is caused only from sticking. For a good FSW practice, the material should be adequately softened for flow, the tool should have adequate grip on the plasticised material and the total torque and traverse force should not be excessive. Experimental investigations[89] have shown that only a tool with an optimal shoulder diameter results in the highest strength of the AA 6061 FSW joints. Although the need to determine an optimum shoulder diameter has been recognised in the literature, the search for an appropriate principle for the determination of an optimum shoulder diameter is just beginning.

Table 7 Properties of common tool materials

	Coefficient of thermal expansion/10^{-6} K^{-1}	Thermal conductivity/ W m^{-1} K^{-1}	Yield strength/MPa	Hardness/HV	Remarks
pcBN	4·6–4·9 (Ref. 61)	100–250 (Ref. 61)		2600–3500	Pros: high hardness; high temperature strength Cons: susceptible to crack; wear may be enhanced by chemical reactions with Ti; high cost
cp-W	~4·6 at 20–1000°C (Ref. 159)	167 at 20°C (Ref. 159) 111 at 1000°C	~100 at 1000°C (Ref. 58)	360–500 (Ref. 159)	Pros: high temperature strength Cons: low toughness at room temperature; less strong than W alloys, WC, or pcBN
W–25 wt-%Re		55–65 (Ref. 53)	~500–800 at 1000°C (Ref. 58)		Pros: higher strength than W; tougher and easier to machine than ceramics
WC	4·9–5.1 (Ref. 61)	95 (Ref. 61)		1300–1600 (Ref. 61)	Pros: high temperature strength; high hardness Cons: wear due to oxidation at high temperatures; addition of Cr_3C_2 prevents oxidation
4340 Steel	11·2–14·3 (Ref. 61)	48 (Ref. 61)		280 (Ref. 61)	Pros: low thermal conductivity Cons: high temperature strength is not very high; possible alloying with Ti
TiC	8·31 (Ref. 160)	5–31 (Ref. 160)	20 000 (Ref. 160)	2800–3400 (Ref. 160)	Pros: high hardness; high temperature strength Cons: susceptible to crack
Si_3N_4	3·9 at 20°C 6·7 at 1000°C (Ref. 161)	20–70 (Ref. 162)		1580	Pros: high hardness; high temperature strength Cons: susceptible to crack; decomposes at high temperatures

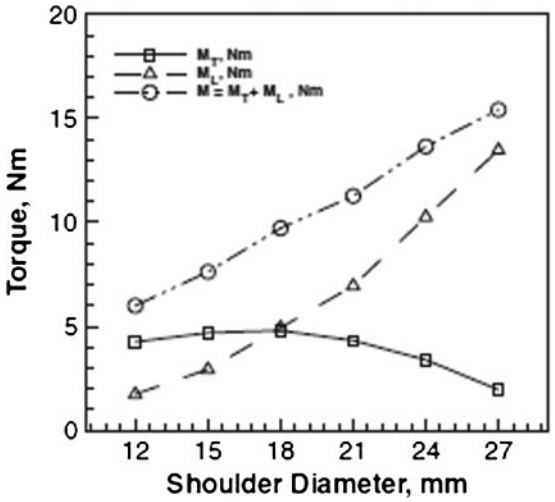

2 Variation of sliding torque, sticking torque and total torque with shoulder diameter[90]

Arora *et al.*[90] proposed a method to determine optimal shoulder diameter by considering the sticking M_T and sliding M_L components of torque. These torques are calculated based on the tool geometry, flow stresses in workpiece and the axial pressure as

$$M_T = \oint_A r_A \times (1-\delta)\tau \mathrm{d}A \quad (1)$$

$$M_L = \oint_A r_A \delta \mu_f P_N \mathrm{d}A \quad (2)$$

where δ and μ_f are spatially variable fractional slip and coefficient of friction between the tool and the workpiece respectively, τ is the shear stress at yielding, r_A is the distance of any infinitesimal area element $\mathrm{d}A$ from the tool axis and P_N is the axial pressure. δ and μ_f were given as functions of tool rotation speed and the radial distance from tool axis.[91,92] The total torque M is the sum of the sticking and sliding components of torques. The required spindle power was calculated from the total torque as

$$P = \omega(M_T + M_L) \quad (3)$$

Figure 2 shows that for the welding of AA 6061, the sliding torque continuously increases with shoulder diameter because of the larger tool/workpiece interfacial area. However, the sticking torque increases, reaches a maximum and then decreases. This behaviour can be understood from equation (1) that shows two important factors that affect the sticking torque. First, with increase in temperature, the flow stress τ decreases and at the same time the area increases with shoulder diameter. The product of these two opposing factors leads to a maximum in the sticking torque versus shoulder diameter plot which indicates the maximum grip of the shoulder on the plasticised material. Any further increase in the shoulder diameter results in decreased grip of the tool on the material, higher total torque and higher power requirement. For these reasons, Arora *et al.*[90] suggested that the optimum shoulder diameter should correspond to the maximum sticking torque for a given set of welding parameters and workpiece material.

The principle of optimising shoulder diameter from a consideration of maximising tool's grip on the plasticised material remains to be tested on harder materials such as steels and titanium alloys.

Shoulder surface

The nature of the tool shoulder surface is an important aspect of tool design. Hirasawa *et al.*[78] studied flat, convex and concave tool shoulders, and cylindrical, tapered, inverse tapered and triangular pin geometries. They found that triangular pins with concave shoulders resulted in high strength spot welds. Sorensen and Nielsen[86] examined the role of geometric parameters of convex shoulder step spiral (CS4) tools and identified the radius of curvature of the tool shoulder and pitch of the step spiral as important geometric parameters. Microstructure, geometry and failure mode of a weld may be significantly altered if the tool shoulder chosen is concave rather than flat.[93,94] The finite element modelling results of Li *et al.*[95] showed that the shoulder surface angle affected the axial force depending on the tool pin radius. A convex shoulder with scrolls was shown to improve FSW process stability.[96] It was argued that when a convex scroll shoulder is used in constant axial force mode, any increase in plunge depth from its normal value results in greater contact area between the shoulder and the workpiece. As a result, the axial pressure is reduced and the plunge depth decreases to its original value. Similarly, any decrease in the plunge depth lowers the shoulder/workpiece contact area resulting in higher axial pressure and a consequent return of the plunge depth to its normal value. Therefore, the FSW process with convex scroll shoulder tends to be stable with a nearly constant plunge depth. Cederqvist *et al.*[96] found that the convex scroll shoulder resulted in minimum flash and no defects as opposed to concave shoulder which resulted in medium flash and some defects. It has been suggested[97,98] that the conventional rotating shoulder tools can result in high thermal gradients and high surface temperatures during FSW of low thermal conductivity alloys leading to deterioration of weld quality. A stationary shoulder friction stir welding process has been developed by The Welding Institute in which the non-rotating shoulder slides on the workpiece surface as the rotating pin moves forward.[97,98]

Pin (probe) geometry

The shape of the tool pin (or probe) influences the flow of plasticised material and affects weld properties.[8,71,77,87,88,99] Kumar and Kailas[100] suggested that while the tool shoulder facilitated bulk material flow the pin aided a layer by layer material flow. Figure 3 shows the shapes of some of the commonly used tool pins. A triangular or 'trifluted' tool pin increases the material flow compared with a cylindrical pin.[78] The axial force on the workpiece material and the flow of material near the tool are affected by the orientation of threads on the pin surface.[101] Fujii *et al.*[82] achieved defect free welds in softer alloys such as AA 1050 using a columnar tool pin without any thread. They suggested that a triangular prism shaped tool pin would be suitable for harder alloys such as AA 5083. Zhao *et al.*[102] used columnar and tapered pins – both with and without threads – and observed that the tapered pin profile with screw thread produced welds

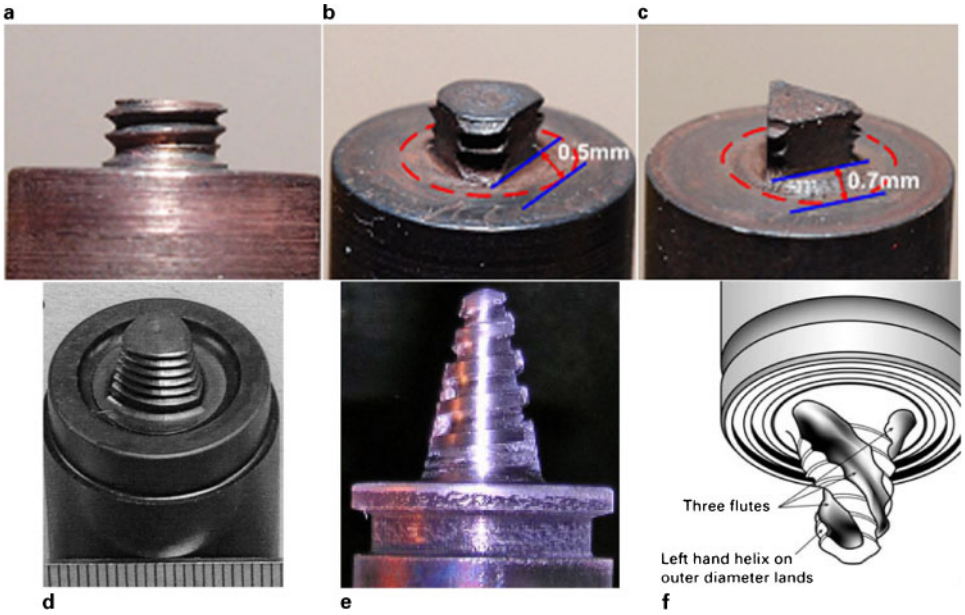

a cylindrical threaded;[79] *b* three flat threaded 1;[79] *c* triangular;[79] *d* Trivex;[133] *e* threaded conical;[109] *f* schematic of a triflute[109]

3 Commonly used tool pin geometries

with the minimum defects in AA 2014. Hattingh *et al.*[81] observed that a trifluted tapered pin with a thread pitch of around 10% of the pin diameter and 15% of plate thickness produced defect free welds. Colegrove and Shercliff[103] compared the computed material flow fields resulting from the use of a triangular tool with convex surfaces (Trivex) and a Triflute tool and suggested that the latter increased the downward force due to its strong augering action. Features such as threads and flutes on the pin are believed to increase heat generation rate due to larger interfacial area, improve material flow and affect the axial and transverse forces. Mahmoud *et al.*[104] studied the friction stir processing of SiC reinforced aluminium composite using four tool shapes – circular without thread, circular with thread, triangular and square. The square probe resulted in more homogeneous distribution of SiC particles than the other tools whereas circular tool experienced much less wear than the flat faced tools. Elangovan *et al.*[105] studied five tool profiles – straight cylindrical, threaded cylindrical, tapered cylindrical, square and triangular – for the welding of AA 6061 aluminium alloy and found that the square pin profiled tools produced defect free welds for all the axial forces used. Lammlein *et al.*[106] observed significant reduction in process forces with a conical shoulderless tool that could also be used to weld plates of variable thicknesses. However, process stability, weld line alignment and weld root defects were important issues.

Insufficient material flow on the advancing side, particularly at low processing temperatures, often results in formation of defects such as wormholes.[107,108] The 'restir' tool, which periodically reverses its direction of rotation, was devised by The Welding Institute to address this issue.[109] An increase in the angle between the conical surface of the pin and its axis leads to a more uniform temperature distribution along the vertical direction and helps in reducing distortion.[110] Buffa *et al.*[110] showed that an increase in the pin angle increased peak temperature. Furthermore, it has been suggested[110] that the helical motion of a conical pin pushes the material downwards in the front and upwards in the rear. The improved material flow results in more uniform properties across the workpiece thickness.[110] As a result, tapered tools are preferred when welding thick sheets.

Tools used for friction stir spot welding (FSSW) experience only torsion due to rotational motion as opposed to tools used for FSW that experience both bending moment and torsion due to linear and rotational motion respectively. Despite the differences between FSSW and FSW, the tools used for the two processes are similar. Tozaki *et al.*[111] used tools with cylindrical pins with three different pin lengths to understand the effect of tool geometry on microstructure and static strength in friction stir spot welded aluminium alloys. They showed that the tensile shear strength of the welds increased when longer tool pins were used. Yang *et al.*[112] used tool pins with circular and triangular cross-sections for welding of AZ31 Mg sheets in lap joint configuration and used Cu as tracer material to study material flow. Hirasawa *et al.*[78] used the particle method to analyse material flow in lap joints, for various shoulder and pin geometries, by tracking the position of reference particles originally located at a fixed distance from the top surface. For cylindrical pin tool, material flow is upwards near the pin periphery whereas the material beneath the shoulder is pushed downwards due to the axial force from the shoulder. Thus, moving away from the pin periphery, the reference line of particles curves upwards and then bends down resulting in a 'hook' formation.[78,113] Characteristics of hook regions have been found to be related to mechanical properties of lap joints.[85,93,94,113–116] Hirasawa *et al.*[78] found that the nature of hook formation was influenced by the pin and shoulder geometries. Choi *et al.*[67] used cylindrical pin tools made of two different materials to evaluate the frictional wear during FSSW of low carbon steel. Tozaki *et al.*[117] proposed a tool without a pin in order to avoid the hole commonly left behind at the centre of an FSSW. When this tool was used for lap

joints in 2 mm thick sheets of AA 6061-T4, welds with shear strength comparable with those made with a conventional tool were obtained. The shoulder plunge was an important parameter as the stirring action was achieved by scrolls on the tool shoulder.

Load bearing ability

In an FSW process, the commonly used tool experiences axial, longitudinal and lateral forces due to viscous and inertial effects.[118] As the tool rotates inside the workpiece, it experiences an axial force that tends to lift the tool and is countered by the applied axial force through the tool shoulder. The longitudinal forces on the FSW tool result from the linear motion of the tool through the workpiece. The rotation of the tool combined with the linear motion results in an asymmetric flow field around the tool leading also to a lateral force on the tool in the direction perpendicular to that of the linear motion due to Magnus effect.[118,119] As the workpiece comes in contact with first the pin, and then the shoulder during the initial plunge, the forces acting on the tool vary significantly due to the combination of work hardening (under axial compression and shear) and softening due to heat generation.[118,120] After the plunge, as the tool traverses some distance in the workpiece, the forces on tool stabilise at a value which is generally lower than the peak forces during the plunge state.[118,120] Therefore, tools are subjected to more severe stresses during the initial plunge compared with the linear traverse stage. Tools, especially those made of brittle materials such as pcBN, are more likely to fail in the initial plunge stage than later in the welding process. Preheating of the workpiece is sometimes used to lower the tool stresses during the initial plunge.

The forces and torques acting on the tool are important for several reasons. First, a larger torque corresponds to a greater power requirement for the FSW process.[118] Second, tool deformation and wear are enhanced with increasing load on the tool leading to greater processing cost due to more frequent tool replacement. Third, tool wear may lead to contamination of the weld and deterioration of the joint properties.

Atharifar *et al.*[118] modelled FSW process with a threaded tool pin and calculated the axial, longitudinal and lateral forces on the pin and the shoulder. Both experimental and calculated results showed that the axial forces increased with increasing rotational speed and decreasing tool travel speed. However, the computed results of axial force were not in good agreement with the corresponding measured values except for a small range of angular velocities. Increase in rotational speed and decrease in tool travel speed resulted in decrease in the calculated longitudinal forces on both the tool pin and the tool shoulder. The decrease in the longitudinal force with increasing rotational speed was attributed to the higher heat generation rate and, consequently, lower flow stress. The effect of travel speed on the longitudinal force was attributed to the variation in the dynamic pressure distribution along the welding direction. Both the lateral and the axial forces were influenced much more significantly by the rotational speed compared with the travel speed. The axial, longitudinal and lateral forces acting on the tool shoulder were found to be much larger than the corresponding forces on the tool pin. The calculated moments were high at low rotational and high travel speeds.

The effects of travel and rotational speeds on the forces experienced by FSW tool are compiled in Table 8. The legend $+/-$ in a cell signifies that increase in the column parameter results in an increase/decrease in the corresponding row parameter, and ($\sim$) signifies weak or no effect. The power requirement, calculated as angular velocity times the total torque on the tool, increases significantly with increasing rotational speed. The effect of travel speed is significant only at high rotational speed, where the increase in travel speed requires increased power.

Sorensen and Stahl[120] measured the longitudinal forces on the tool for varying pin lengths at constant pin diameter and vice versa. The longitudinal force on the tool was found to decrease with decreasing pin length and reach a limiting value for a very small pin length (Fig. 4). The limiting longitudinal force was taken as the force experienced by the tool shoulder. Assuming that the longitudinal force on the tool shoulder was independent of the pin length, the force on tool pin was calculated as the difference between the total longitudinal force and the limiting force on the tool shoulder. For pin lengths smaller than 5·6 mm, the total longitudinal force on the tool pin varied as the quadratic power of the pin length, and the pin force increased linearly along its length with distance from the tool shoulder. However, no specific influence of pin diameter on longitudinal pin force was observed.

Since the tool pin is structurally much weaker than the tool shoulder, the susceptibility of an FSW tool to

Table 8 Effect of travel speed and rotational speed on moment and forces*[118]

		Travel speed	Rotational speed
On pin	Longitudinal force	+	−
	Axial force	~	+
	Lateral force	~	+
	Moment about tool axis	~	−
On shoulder	Longitudinal force	+	−
	Axial force	−	+
	Lateral force	~	+
	Moment about tool axis	~	−
Total	Longitudinal force	+	−
	Axial force	−	+
	Lateral force	~	+
	Moment about tool axis	+	−

*Symbols + (−) indicate that an increase in the welding parameter results in larger or smaller values of the corresponding force or moment. Symbol ~ signifies weak or no effect.

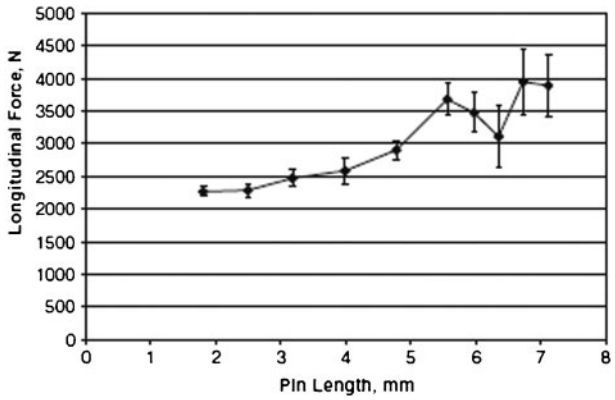

4 Total longitudinal force on pin as function of pin length[120]

deform, wear and/or break will ultimately depend on the resultant stress experienced by the pin. In order to evaluate the possible performance of a pin with a specific geometry, the maximum stress on the pin should be estimated and compared with the tool material shear strength at the corresponding working temperature. Arora *et al.*[121] calculated the torsion and bending stresses experienced by the tool pin due to the rotational and linear motions as functions of process variables and typical pin dimensions.

The three-dimensional material flow and temperature field model given by Nandan *et al.*[122–125] was used for the calculation of the traverse force on the tool pin F_P

$$F_P = \int_0^L \int_0^{2\pi} \sigma(r)\,\mathrm{d}\theta\,\mathrm{d}L \tag{4}$$

where σ is the temperature compensated yield strength of the deforming material around the tool, r is the average pin radius and L is the length of the pin. The traverse force on the tool pin was used to calculate the bending moment and the corresponding normal and shear stresses. Figure 5 shows a two-dimensional schematic diagram of traverse forces on a cylindrical tool pin. The traverse force increases with distance along the pin length because of higher flow stresses at lower temperatures further away from the tool shoulder.

Considering a typical two-dimensional section of a cylindrical tool pin at a distance z_1 from the root of the pin, the bending stress σ_B may be computed as[121]

$$\sigma_B = \frac{4\cos\theta}{\pi r^3} \int_{z_1}^{L} z q(z)\,\mathrm{d}z \tag{5}$$

where $q(z)$ is the traverse force distribution on the tool pin, r is local pin radius and L is the pin length. The shear stress τ_B due to the bending is expressed as

$$\tau_B = \frac{4}{3}\frac{\sin^2\theta}{\pi r^2} \int_{z_1}^{L} q(z)\,\mathrm{d}z \tag{6}$$

The shear stress τ_T due to the torque is computed as

$$\tau_T = \frac{2}{\pi r^3} \oint_A \tau(1-\delta) r_A\,\mathrm{d}A \tag{7}$$

The maximum possible shear stress at any point on the pin with a circular cross-section can be given as

$$\tau_{max} = \left[\left(\frac{\sigma_B}{2}\right)^2 + (\tau_B + \tau_T \sin\theta)^2 + (\tau_T \cos\theta)^2\right]^{1/2} \tag{8}$$

The maximum shear stress τ_{max} calculated from equation (8) multiplied with a reasonable value of factor of safety should be smaller than the shear yield strength of the tool material at typical stir zone working temperature to avoid tool failure during welding. The shear strength is dependent on the tool pin material while the pin geometry affects the stresses due to bending and torsion. The traverse force on the pin increases with increasing pin length[121] as shown in Fig. 6. The maximum possible shear stresses in the pin decrease strongly with increasing pin radius as given by equations (1)–(4). As the pin length is often determined by the plate thickness, a minimum pin radius may be specified by considering the maximum stresses in the pin and the strength of tool material under given processing conditions. For the welding of thicker plates, a larger pin radius may be required to avoid tool breakage due to larger traverse forces. The nature of equations (5)–(8) also shows that the tool, in particular the tool pin, experiences a highest and a lowest value of τ_{max} along each cross-sectional plane during one complete rotation (θ=0–2π) leading to the imposition of a dynamic load cycle. Although the extent of such dynamic load cycle may be smaller in comparison with the steady thermal and mechanical loads, the former can also contribute to the vibration and subsequent failure of the tools. Since the maximum bending moments in the pin are present

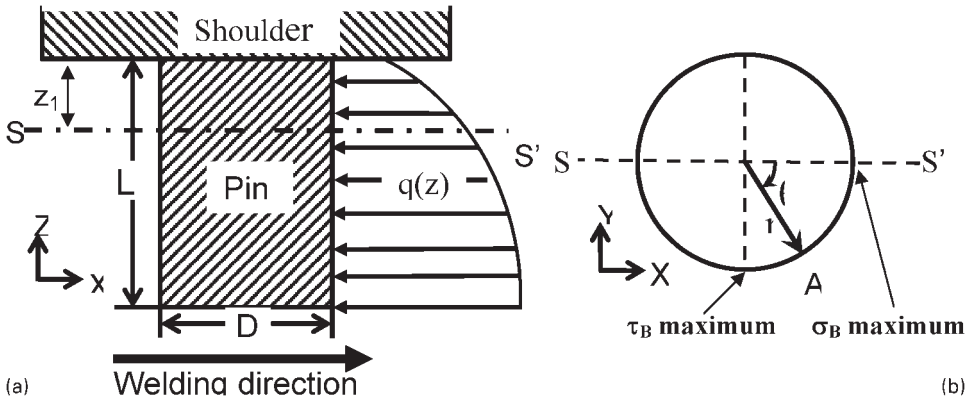

5 Schematic layout of *a* cylindrical pin and *b* cross-section along S–S'

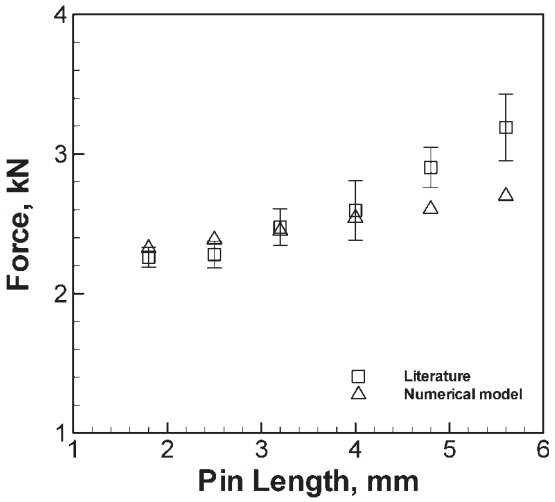

6 Variation of traverse force on pin with change in pin length[120,121]

close to the pin–shoulder joint, it is important to have larger cross-sections at locations closer to the shoulder compared with locations farther away. As the pin radius becomes larger, more and more material needs to be moved around to fill the gap. In addition to requiring more power, it may also lead to poor weld quality if the gap is not adequately filled. Both weld quality and tool failure need to be considered for the design of pin geometry.

Tool wear, deformation and failure

The rotation and translation of tool through the workpiece result in its wear. The FSW tool may also deform plastically due to a reduction in yield strength at elevated temperatures in an environment of high loads. Therefore, FSW tools for welding of high strength materials such as steels are often liquid cooled.[7] When the stresses are higher than the load bearing ability of the tool, failure may occur.

Not many detailed studies have been done on the tool wear in FSW but diffusion and abrasion are the expected wear mechanisms. Reaction of the tool material with its environment, including both the workpiece and the surrounding gases, is also expected to contribute to the tool wear. Ellingham diagrams for oxide formation, shown in Fig. 1, indicate the relative propensity of oxidation of several pure metals from a thermodynamic point of view and similar diagrams may be constructed for nitride formation. Furthermore, there is a need to identify the possibility of interaction of the tool material with the workpiece by diffusion and chemical reaction in model tests and actual FSW processes. Depending on the results, a particular tool material may be a good choice for one workpiece material but not for another of similar physical properties. Some such studies for wear in cutting operations have been done for the interaction of pcBN with steels.[45–49] Wear through abrasion is particularly significant in the presence of a harder second phase such as in AMCs.[68] Fig. 7 shows severe initial wear of a threaded 01 AISI oil-hardened steel tool during FSW of Al6061 + 20 vol.-%Al_2O_3 AMC. However, it has been reported that the wear rates decrease considerably after the initial wear and the smoothed (or self-optimized) tools, similar to those shown in Fig. 7, can continue producing good quality welds.[9,11,26]

A high strength material, such as W or pcBN, is chosen to reduce the plastic deformation of tool. Strength may be further increased through microstructural changes such as restricting the grain size in tungsten through addition of lanthanum or lanthanum oxide. Alloying with Re increases the yield strength and decreases the ductile to brittle transition temperature of tungsten.[58] High fracture toughness is important to reduce the likelihood of sudden brittle failure. Some work has been done to develop new grades of pcBN with higher fracture toughness and greater tool life.[41,50,126–128]

Compared with the tool shoulder, the tool pin suffers much more severe wear and deformation, and the tool failures almost always occur in the pin. This is expected due to several reasons. First, the tool pin is completely immersed in the workpiece and, therefore, has to face

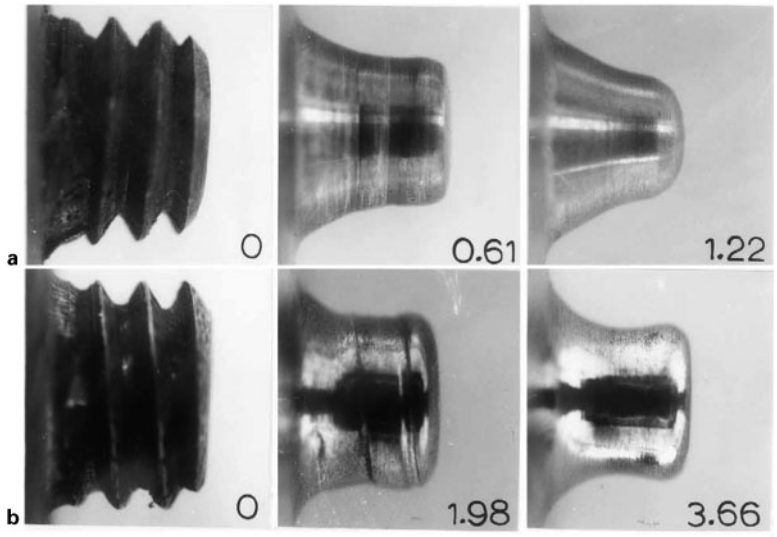

7 Evolution of tool shape due to wear in FSW of Al 6061 + 20 vol.-%Al_2O_3 metal matrix composite with 01 AISI oil hardened steel tool at 1000 rev min^{-1} and travel speeds of *a* 3 mm s^{-1} and *b* 9 mm s^{-1}: distances traversed by tool in metres are indicated[9]

more resistance to its motion compared with the tool shoulder, only a small part of which is inside the workpiece. Second, since most of the heat is generated near the shoulder/workpiece interface, resistance to the motion of the shoulder is much smaller than that to the pin. Consequently, a pin profile that enhances downward flow of the hotter and softer material from the top should decrease the forces on the pin. Third, the pin has much lower load bearing capabilities than the shoulder due to the high stresses resulting in the former from a combination of torsion and bending stresses in its typically slender shape. One consequence of the above observation is that composite tools[58] with harder, wear resistant material (e.g. pcBN or WC) for pin and relatively softer material (e.g. W–Re alloy) for shoulder may be an attractive option for enhancing tool life and reducing tool costs.

In some cases, special techniques have been used to reduce tool wear.[4,7] For example, in lap joints of dissimilar materials, the tool is placed in the softer material and contact between the tool and the harder material is avoided to reduce the tool wear.[18,24,63,129] Welding of dissimilar metals[23] in butt joint configuration by offsetting the tool towards the softer alloy side needs to be more thoroughly tested. Some of the other strategies to reduce tool wear are to weld at lower welding speeds, preheat the workpiece to reduce its mechanical resistance, preheat the tool above the ductile to brittle transition temperature and use sufficient inert gas cover.[4,7] However, the commercial applicability of these techniques remains to be tested.

Tool cost

While the energy cost for the FSW of aluminium alloys is significantly lower than that for the fusion welding processes,[130] the process is not cost effective for the FSW of hard alloys. Tools made of pcBN are often used for the welding of hard materials. However, pcBN is expensive due to high temperatures and pressures required in its manufacture. Santella *et al.*[33] did an approximate cost benefit analysis for FSSW with a pcBN tool versus resistance spot welding (RSW) of DP 780 steel. The equipment and utility costs for FSSW were assumed to be 90 and 30% respectively of the costs in RSW; however, they did not report the dollar amounts of these costs. They further assumed that a typical RSW tool tip lasts 5000 welds and costs \$0·65 per tip. Considering the costs involved with equipment, utility and the tool, they estimated that in order for the FSSW to be cost competitive with respect to RSW, each FSSW tool, costing ~\$100, needs to make 26 000 spot welds. Since the cost of each pcBN tool was significantly greater than \$100 and typical tool life was between 500 and 1000 welds, they suggested lowering tool costs as an important need. Feng *et al.*[131] produced over 100 friction stir spot welds on dual phase steel (ultimate tensile strength 600 MPa) and martensitic steel (ultimate tensile strength 1310 MPa) without noticeable degradation of the pcBN tool.

Several FSSW tools have been developed with Si_3N_4, TiB_2 and pcBN.[127] The costs of Si_3N_4 and TiB_2 tools were less than 25% of the cost of pcBN tools.[127] Machine loads for Si_3N_4 tools were ~75% of that for pcBN tools and the two tools resulted in similar joint strengths.[127] Tools of W–Re or W–La alloys are relatively less expensive than that of pcBN tool but suffer considerably more wear compared with superabrasives due to their relatively lower high temperature strength and hardness.

Concluding remarks

Cost effective and long life tools are available for the FSW of aluminium and other soft alloys. They are needed but not currently available for the commercial application of FSW to high strength materials. Tool material properties such as strength, fracture toughness, hardness, thermal conductivity and thermal expansion coefficient affect the weld quality, tool wear and performance. Reactivity of tool material with oxygen from the atmosphere and with the workpiece is also an important consideration. pcBN and W based alloys are important candidate materials for the FSW of high strength materials. High strength, hardness and high temperature stability of pcBN allow much smaller wear compared with other tools. Low fracture toughness and high cost of pcBN are issues that need attention. W based alloys, although not as hard and wear resistant, are more affordable options and have been used to weld steels and Ti alloys in a limited scale. There is also an interest in Si_3N_4 as a prospective tool material because it had produced welds comparable with pcBN tools at a much lower cost. Further developments in FSW tool materials are required to address the problem of high tool cost with low tool life during welding of harder alloys.

Heat generation rate and plastic flow in the workpiece are affected by the shape and size of the tool shoulder and pin. Although the tool design affects weld properties, defects and the forces on the tool, they are currently designed empirically by trial and error. Work on the systematic design of tools using scientific principles is just beginning. Examples of recent studies include calculation of flow fields for different tool geometries and the calculation of tool shoulder dimensions based on the tool's grip of the plasticised material. The pin cross-sectional geometry and surface features such as threads influence the heat generation rates, axial forces on the tool and material flow. Tool wear, deformation and failure are also much more prominent in the tool pin compared with the tool shoulder. The axial, longitudinal and lateral forces on the tool can be calculated as functions of process parameters, or evaluated from the measured data. Estimation of the load bearing ability of the tool pin is needed considering the maximum stresses in the tool pin due to combined effects of bending and torsion. There is a need for concerted research efforts towards development of cost effective durable tools for commercial application of FSW to hard engineering alloys.

References

1. W. M. Thomas, E. D. Nicholas, J. C. Needham, M. G. Murch, P. Templesmith and C. J. Dawes: 'Friction stir butt welding', US Patent 5460317, 1995.
2. C. J. Dawes and W. M. Thomas: 'Friction stir process welds aluminum alloys', *Weld. J.*, 1996, **75**, (3), 41–45.
3. E. D. Nicholas and W. M. Thomas: 'A review of friction processes for aerospace applications', *Int. J. Mater. Prod. Technol.*, 1998, **13**, (1–2), 45–55.

4. W. M. Thomas, P. L. Threadgill and E. D. Nicholas: 'Feasibility of friction stir welding steel', *Sci. Technol. Weld. Join.*, 1999, **4**, (6), 365–372.
5. W. M. Thomas: 'Friction stir welding – recent developments', *Mater. Sci. Forum*, 2003, **426–432**, 229–236.
6. H. Bhadeshia and T. DebRoy: 'Critical assessment: friction stir welding of steels', *Sci. Technol. Weld. Join.*, 2009, **14**, (3), 193–196.
7. G. Cam: 'Friction stir welded structural materials: beyond Al-alloys', *Int. Mater. Rev.*, 2011, **56**, (1), 1–48.
8. R. S. Mishra and Z. Y. Ma: 'Friction stir welding and processing', *Mater. Sci. Eng. A*, 2005, **50**, (1–2), 1–78.
9. R. A. Prado, L. E. Murr, K. F. Soto and J. C. McClure: 'Self-optimization in tool wear for friction-stir welding of Al 6061+20% Al2O3 MMC', *Mater. Sci. Eng. A*, 2003, **A349**, (1–2), 156–165.
10. R. A. Prado, L. E. Murr, D. J. Shindo and K. F. Soto: 'Tool wear in the friction-stir welding of aluminum alloy 6061+20% Al_2O_3: a preliminary study', *Scr. Mater.*, 2001, **45**, (1), 75–80.
11. G. J. Fernandez and L. E. Murr: 'Characterization of tool wear and weld optimization in the friction-stir welding of cast aluminum 359+20% SiC metal-matrix composite', *Mater. Charact.*, 2004, **52**, (1), 65–75.
12. W. B. Lee, Y. M. Yeon and S. B. Jung: 'Joint properties of friction stir welded AZ31B-H24 magnesium alloy', *Mater. Sci. Technol.*, 2003, **19**, (6), 785–790.
13. N. A. Rodriguez, E. Almanza, C. J. Alvarez and L. E. Murr: 'Study of friction stir welded A319 and A413 aluminum casting alloys', *J. Mater. Sci.*, 2005, **40**, (16), 4307–4312.
14. H. Nami, H. Adgi, M. Sharifitabar and H. Shamabadi: 'Microstructure and mechanical properties of friction stir welded Al/Mg2Si metal matrix cast composite', *Mater. Des.*, 2011, **32**, (2), 976–983.
15. R. K. R. Singh, C. Sharma, D. K. Dwivedi, N. K. Mehta and P. Kumar: 'The microstructure and mechanical properties of friction stir welded Al–Zn–Mg alloy in as welded and heat treated conditions', *Mater. Des.*, 2011, **32**, (2), 682–687.
16. S. Rajakumar, C. Muralidharan and V. Balasubramanian: 'Influence of friction stir welding process and tool parameters on strength properties of AA7075-T-6 aluminium alloy joints', *Mater. Des.*, 2011, **32**, (2), 535–549.
17. W. M. Thomas, E. D. Nicholas, E. R. Watts and D. G. Staines: 'Friction based welding technology for aluminium', *Mater. Sci. Forum*, 2002, **396–402**, 1543–1548.
18. C. Y. Lee, D. H. Choi, Y. M. Yeon and S. B. Jung: 'Dissimilar friction stir spot welding of low carbon steel and Al–Mg alloy by formation of IMCs', *Sci. Technol. Weld. Join.*, 2009, **14**, (3), 216–220.
19. A. Elrefaey, M. Gouda, M. Takahashi and K. Ikeuchi: 'Characterization of aluminum/steel lap joint by friction stir welding', *J. Mater. Eng. Perform.*, 2005, **14**, (1), 10–17.
20. T. Chen: 'Process parameters study on FSW joint of dissimilar metals for aluminum-steel', *J. Mater. Sci.*, 2009, **44**, (10), 2573–2580.
21. T. P. Chen and W. B. Lin: 'Optimal FSW process parameters for interface and welded zone toughness of dissimilar aluminium-steel joint', *Sci. Technol. Weld. Join.*, 2010, **15**, (4), 279–285.
22. T. DebRoy and H. Bhadeshia: 'Friction stir welding of dissimilar alloys – a perspective', *Sci. Technol. Weld. Join.*, 2010, **15**, (4), 266–270.
23. U. Dressler, G. Biallas and U. A. Mercado: 'Friction stir welding of titanium alloy TiAl6V4 to aluminium alloy AA2024-T3', *Mater. Sci. Eng. A*, 2009, **A526**, (1–2), 113–117.
24. M. P. Miles, Z. Feng, K. Kohkonen, B. Weickum, R. Steel and L. Lev: 'Spot joining of AA 5754 and high strength steel sheets by consumable bit', *Sci. Technol. Weld. Join.*, 2010, **15**, (4), 325–330.
25. C. Meran and V. Kovan: 'Microstructures and mechanical properties of friction stir welded dissimilar copper/brass joints', *Materialwiss. Werkstofftech.*, 2008, **39**, (8), 521–530.
26. D. J. Shindo, A. R. Rivera and L. E. Murr: 'Shape optimization for tool wear in the friction-stir welding of cast Al359-20% SiC MMC', *J. Mater. Sci.*, 2002, **37**, (23), 4999–5005.
27. S. H. C. Park, Y. S. Sato, H. Kokawa, K. Okamoto, S. Hirano and M. Inagaki: 'Rapid formation of the sigma phase in 304 stainless steel during friction stir welding', *Scr. Mater.*, 2003, **49**, (12), 1175–1180.
28. S. H. C. Park, Y. S. Sato, H. Kokawa, K. Okamoto, S. Hirano and M. Inagaki: 'Microstructural characterisation of stir zone containing residual ferrite in friction stir welded 304 austenitic stainless steel', *Sci. Technol. Weld. Join.*, 2005, **10**, (5), 550–556.
29. M. P. Miles, T. W. Nelson, R. Steel, E. Olsen and M. Gallagher: 'Effect of friction stir welding conditions on properties and microstructures of high strength automotive steel', *Sci. Technol. Weld. Join.*, 2009, **14**, (3), 228–232.
30. Y. Zhang, Y. S. Sato, H. Kokawa, S. H. C. Park and S. Hirano: 'Stir zone microstructure of commercial purity titanium friction stir welded using pcBN tool', *Mater. Sci. Eng. A*, 2008, **A488**, (1–2), 25–30.
31. Y. S. Sato, H. Yamanoi, H. Kokawa and T. Furuhara: 'Microstructural evolution of ultrahigh carbon steel during friction stir welding', *Scr. Mater.*, 2007, **57**, 557–560.
32. Y. S. Sato, T. W. Nelson, C. J. Sterling, R. J. Steel and C. O. Pettersson: 'Microstructure and mechanical properties of friction stir welded SAF 2507 super duplex stainless steel', *Mater. Sci. Eng. A*, 2005, **A397**, (1–2), 376–384.
33. M. Santella, Y. Hovanski, A. Frederick, G. Grant and M. Dahl: 'Friction stir spot welding of DP780 carbon steel', *Sci. Technol. Weld. Join.*, 2010, **15**, (4), 271–278.
34. S. Park, Y. Sato, H. Kokawa, K. Okamoto, S. Hirano and M. Inagaki: 'Boride formation induced by pcBN tool wear in friction-stir-welded stainless steels', *Metall. Mater. Trans. A*, 2009, **40A**, (3), 625–636.
35. Y. Hovanski, M. L. Santella and G. J. Grant: 'Friction stir spot welding of hot-stamped boron steel', *Scr. Mater.*, 2007, **57**, (9), 873–876.
36. Y. S. Sato, N. Harayama, H. Kokawa, H. Inoue, Y. Tadokoro and S. Tsuge: 'Evaluation of microstructure and properties in friction stir welded superaustenitic stainless steel', *Sci. Technol. Weld. Join.*, 2009, **14**, (3), 202–209.
37. C. D. Sorensen and T. W. Nelson: 'Friction stir welding of ferrous and nickel alloys', in 'Friction stir welding and processing', (ed. R. S. Mishra and M. W. Mahoney), Vol. 6, 111–121; 2007, Materials Park, OH, ASM International.
38. B. K. Agarwala, B. P. Singh and S. K. Singhal: 'Synthesis and characterization of polycrystalline sintered compacts of cubic boron-nitride', *J. Mater. Sci.*, 1986, **21**, (5), 1765–1768.
39. H. Sumiya, S. Uesaka and S. Satoh: 'Mechanical properties of high purity polycrystalline cBN synthesized by direct conversion sintering method', *J. Mater. Sci.*, 2000, **35**, (5), 1181–1186.
40. S. Gimenez, O. van der Biest and J. Vleugels: 'The role of chemical wear in machining iron based materials by PCD and PCBN super-hard tool materials', *Diam. Relat. Mater.*, 2007, **16**, (3), 435–445.
41. M. Collier, R. Steel, T. Nelson, C. Sorensen and S. Packer: 'Grade development of polycrystalline cubic boron nitride for friction stir processing of ferrous alloys', *Mater. Sci. Forum*, 2003, **426–432**, 3011–3016.
42. M. P. D'Evelyn and T. Taniguchi: 'Elastic properties of translucent polycrystalline cubic boron nitride as characterized by the dynamic resonance method', *Diam. Relat. Mater.*, 1999, **8**, (8–9), 1522–1526.
43. C. A. M. Casanova, N. M. Balzaretti, G. Voronin and J. A. H. da Jornada: 'Experimental study of plastic deformation during sintering of cubic boron nitride compacts', *Diam. Relat. Mater.*, 1999, **8**, (8–9), 1451–1454.
44. T. K. Harris, E. J. Brookes and C. J. Taylor: 'The effect of temperature on the hardness of polycrystalline cubic boron nitride cutting tool materials', *Int. J. Refract. Met. Hard Mater.*, 2004, **22**, (2–3), 105–110.
45. W. Konig and A. Neises: 'Wear mechanisms of ultrahard, nonmetallic cutting materials', *Wear*, 1993, **162**, 12–21.
46. R. M. Hooper, J. I. Shakib and C. A. Brookes: 'Microstructure and wear of TiC cubic BN tools', *Mater. Sci. Eng. A*, 1988, **A106**, 429–433.
47. F. Nabhani: 'Wear mechanisms of ultra-hard cutting tools materials', *J. Mater. Process. Technol.*, 2001, **115**, (3), 402–412.
48. G. Poulachon, A. Moisan and I. S. Jawahir: 'Tool-wear mechanisms in hard turning with polycrystalline cubic boron nitride tools', *Wear*, 2001, **250**, 576–586.
49. M. Zimmermann, M. Lahres, D. V. Viens and B. L. Laube: 'Investigations of the wear of cubic boron nitride cutting tools using Auger electron spectroscopy and X-ray analysis by EPMA', *Wear*, 1997, **209**, (1–2), 241–246.
50. T. W. Nelson: 'Friction stir welds of HSLA steel panels for shipyard applications', Friction Stir Science and Technology (ONR), Book of abstracts, PI Review Meeting, York, PA, USA Oct 2009, page 26.
51. M. Mahoney, T. Nelson, C. Sorensen and S. Packer: 'Friction stir welding of ferrous alloys: current status', *Mater. Sci. Forum*, 2010, **638–642**, 41–46.

52. C. D. Sorensen: 'Evaluation of PCBN pin tool wear during FSW of structural steel', Friction Stir Science and Technology (ONR), Book of abstracts, PI Review Meeting, York, PA, USA Oct 2009, page 30.
53. B. K. Jasthi, W. J. Arbegast and S. M. Howard: 'Thermal expansion coefficient and mechanical properties of friction stir welded invar (Fe–36%Ni)', *J. Mater. Eng. Perform.*, 2009, **18**, (7), 925–934.
54. P. L. Raffo: 'Yielding and fracture in tungsten and tungsten-rhenium alloys', *J. Less Common Met.*, 1969, **17**, (2), 133–149.
55. M. I. Khan, M. L. Kuntz, P. Su, A. Gerlich, T. North and Y. Zhou: 'Resistance and friction stir spot welding of DP600: a comparative study', *Sci. Technol. Weld. Join.*, 2007, **12**, (2), 175–182.
56. B. Thompson and S. S. Babu: 'Tool degradation characterization in the friction stir welding of hard metals', *Weld. J.*, 2010, **89**, (12), 256S–261S.
57. T. Weinberger, N. Enzinger and H. Cerjak: 'Microstructural and mechanical characterisation of friction stir welded 15–5PH steel', *Sci. Technol. Weld. Join.*, 2009, **14**, (3), 210–215.
58. W. Gan, Z. T. Li and S. Khurana: 'Tool materials selection for friction stir welding of L80 steel', *Sci. Technol. Weld. Join.*, 2007, **12**, (7), 610–613.
59. T. Liyanage, J. Kilbourne, A. P. Gerlich and T. H. North: 'Joint formation in dissimilar Al alloy/steel and Mg alloy/steel friction stir spot welds', *Sci. Technol. Weld. Join.*, 2009, **14**, (6), 500–508.
60. T. Leonhardt: 'Properties of tungsten-rhenium and tungsten-rhenium with hafnium carbide', *JOM*, 2009, **61**, (7), 68–71.
61. C. Meran, V. Kovan and A. Alptekin: 'Friction stir welding of AISI 304 austenitic stainless steel', *Materialwiss. Werkstofftech.*, 2007, **38**, 829–835.
62. K. Reshad Seighalani, M. K. Besharati Givi, A. M. Nasiri and P. Bahemmat: 'Investigations on the effects of the tool material, geometry, and tilt angle on friction stir welding of pure titanium', *J. Mater. Eng. Perform.*, 2010, **19**, (7), 955–962.
63. Y. C. Chen and K. Nakata: 'Microstructural characterization and mechanical properties in friction stir welding of aluminum and titanium dissimilar alloys', *Mater. Des.*, 2009, **30**, (3), 469–474.
64. J. Teimournezhad and A. Masoumi: 'Experimental investigation of onion ring structure formation in friction stir butt welds of copper plates produced by non-threaded tool pin', *Sci. Technol. Weld. Join.*, 2010, **15**, (2), 166–170.
65. A. P. Reynolds, W. Tang, T. Gnaupel-Herold and H. Prask: 'Structure, properties, and residual stress of 304L stainless steel friction stir welds', *Scr. Mater.*, 2003, **48**, (9), 1289–1294.
66. A. P. Reynolds, W. Tang, M. Posada and J. DeLoach: 'Friction stir welding of DH36 steel', *Sci. Technol. Weld. Join.*, 2003, **8**, (6), 455–460.
67. D. H. Choi, C. Y. Lee, B. W. Ahn, J. H. Choi, Y. M. Yeon, K. Song, H. S. Park, Y. J. Kim, C. D. Yoo and S. B. Jung: 'Frictional wear evaluation of WC–Co alloy tool in friction stir spot welding of low carbon steel plates', *Int. J. Refract. Met. Hard Mater.*, 2009, **27**, 931–936.
68. H. J. Liu, J. C. Feng, H. Fujii and K. Nogi: 'Wear characteristics of a WC–Co tool in friction stir welding of AC4A + 30 vol%SiCp composite', *Int. J. Mach. Tools Manuf.*, 2005, **45**, (14), 1635–1639.
69. G. Buffa, J. Hua, R. Shivpuri and L. Fratini: 'A continuum based FEM model for friction stir welding – model development', *Mater. Sci. Eng. A*, 2006, **A419**, (1–2), 389–396.
70. P. Edwards and M. Ramulu: 'Effect of process conditions on superplastic forming behaviour in Ti–6Al–4V friction stir welds', *Sci. Technol. Weld. Join.*, 2009, **14**, (7), 669–680.
71. M. K. Yadava, R. S. Mishra, Y. L. Chen, B. Carlson and G. J. Grant: 'Study of friction stir joining of thin aluminium sheets in lap joint configuration', *Sci. Technol. Weld. Join.*, 2010, **15**, (1), 70–75.
72. R. P. Martinho, F. J. G. Silva and A. P. M. Baptista: 'Wear behaviour of uncoated and diamond coated Si3N4 tools under severe turning conditions', *Wear*, 2007, **263**, 1417–1422.
73. R. Ohashi, M. Fujimoto, S. Mironov, Y. S. Sato and H. Kokawa: 'Effect of contamination on microstructure in friction stir spot welded DP590 steel', *Sci. Technol. Weld. Join.*, 2009, **14**, (3), 221–227.
74. W. B. Lee, C. Y. Lee, W. S. Chang, Y. M. Yeon and S. B. Jung: 'Microstructural investigation of friction stir welded pure titanium', *Mater. Lett.*, 2005, **59**, (26), 3315–3318.
75. T. J. Lienert, W. L. Stellwag, B. B. Grimmett and R. W. Warke: 'Friction stir welding studies on mild steel – process results, microstructures, and mechanical properties are reported', *Weld. J.*, 2003, **82**, (1), 1S–9S.
76. S. Mironov, Y. S. Sato and H. Kokawa: 'Microstructural evolution during friction stir welding of Ti–15V–3Cr–3Al–3Sn alloy', *Mater. Sci. Eng. A*, 2010, **A527**, (29–30), 7498–7504.
77. O. Lorrain, V. Favier, H. Zahrouni and D. Lawrjaniec: 'Understanding the material flow path of friction stir welding process using unthreaded tools', *J. Mater. Process. Technol.*, 2010, **210**, (4), 603–609.
78. S. Hirasawa, H. Badarinarayan, K. Okamoto, T. Tomimura and T. Kawanami: 'Analysis of effect of tool geometry on plastic flow during friction stir spot welding using particle method', *J. Mater. Process. Technol.*, 2010, **210**, (11), 1455–1463.
79. N. Sun, Y. H. Yin, A. P. Gerlich and T. H. North: 'Tool design and stir zone grain size in AZ31 friction stir spot welds', *Sci. Technol. Weld. Join.*, 2009, **14**, (8), 747–752.
80. K. Kumar, S. V. Kailas and T. S. Srivatsan: 'Influence of tool geometry in friction stir welding', *Mater. Manuf. Process.*, 2008, **23**, (2), 189–195.
81. D. G. Hattingh, C. Blignault, T. I. van Niekerk and M. N. James: 'Characterization of the influences of FSW tool geometry on welding forces and weld tensile strength using an instrumented tool', *J. Mater. Process. Technol.*, 2008, **203**, (1–3), 46–57.
82. H. Fujii, L. Cui, M. Maeda and K. Nogi: 'Effect of tool shape on mechanical properties and microstructure of friction stir welded aluminum alloys', *Mater. Sci. Eng. A*, 2006, **A419**, (1–2), 25–31.
83. H. Fujii, L. Cui, M. Maeda, Y. S. Sato and K. Nogi: 'Effect of threads on tool in friction stir welding of aluminum alloys', *Adv. Struct. Funct. Mater. Des. Proc.*, 2006, **512**, 389–394.
84. S. J. Vijay and N. Murugan: 'Influence of tool pin profile on the metallurgical and mechanical properties of friction stir welded Al–10 wt.% TiB2 metal matrix composite', *Mater. Des.*, 2010, **31**, (7), 3585–3589.
85. H. Badarinarayan, Q. Yang and S. Zhua: 'Effect of tool geometry on static strength of friction stir spot-welded aluminum alloy', *Int. J. Mach. Tools Manuf.*, 2009, **49**, (2), 142–148.
86. C. D. Sorensen and B. Nielsen: 'Exploring geometry effects for convex scrolled shoulder, step spiral probe FSW tools', Proc. TMS 2009 Annual Meet., San Francisco, CA, USA, February 2009, TMS. Pages: 85–92.
87. P. A. Colegrove and H. R. Shercliff: 'Two-dimensional CFD modelling of flow round profiled FSW tooling', *Sci. Technol. Weld. Join.*, 2004, **9**, (6), 483–492.
88. R. Nandan, T. DebRoy and H. Bhadeshia: 'Recent advances in friction-stir welding – process, weldment structure and properties', *Prog. Mater Sci.*, 2008, **53**, (6), 980–1023.
89. K. Elangovan and V. Balasubramanian: 'Influences of tool pin profile and tool shoulder diameter on the formation of friction stir processing zone in AA6061 aluminium alloy', *Mater. Des.*, 2008, **29**, (2), 362–373.
90. A. Arora, A. De and T. DebRoy: 'Toward optimum friction stir welding tool shoulder diameter', *Scr. Mater.*, 2011, **64**, (1), 9–12.
91. Q. Li and M. Lovell: 'On the critical interfacial friction of a two-roll CWR process', *J. Mater. Process. Technol.*, 2005, **160**, (2), 245–256.
92. R. Nandan, B. Prabu, A. De and T. Debroy: 'Improving reliability of heat transfer and materials flow calculations during friction stir welding of dissimilar aluminum alloys', *Weld. J.*, 2007, **86**, 313S–322S.
93. P. C. Lin, J. Pan and T. Pan: 'Failure modes and fatigue life estimations of spot friction welds in lap-shear specimens of aluminum 6111-T4 sheets. Part 1: Welds made by a concave tool', *Int. J. Fatigue*, 2008, **30**, (1), 74–89.
94. P. C. Lin, J. Pan and T. Pan: 'Failure modes and fatigue life estimations of spot friction welds in lap-shear specimens of aluminum 6111-T4 sheets. Part 2: Welds made by a flat tool', *Int. J. Fatigue*, 2008, **30**, (1), 90–105.
95. H. Li, D. Mackenzie and R. Hamilton: 'Parametric finite-element studies on the effect of tool shape in friction stir welding', *Proc. Inst. Mech. Eng. B: J. Eng. Manuf.*, 2010, **224**, (B8), 1161–1173.
96. L. Cederqvist, C. D. Sorensen, A. P. Reynolds and T. Oberg: 'Improved process stability during friction stir welding of 5 cm thick copper canisters through shoulder geometry and parameter studies', *Sci. Technol. Weld. Join.*, 2009, **14**, (2), 178–184.
97. M. M. Z. Ahmed, B. P. Wynne, W. M. Rainforth and P. L. Threadgill: 'Through-thickness crystallographic texture of stationary shoulder friction stir welded aluminium', *Scr. Mater.*, 2011, **64**, (1), 45–48.
98. M. J. Russell, C. Blignault, N. L. Horrex and C. S. Wiesner: 'Recent developments in the friction stir welding of titanium alloys', *Weld. World*, 2008, **52**, (9–10).

99. D. H. Choi, B. W. Ahn, C. Y. Lee, Y. M. Yeon, K. U. Song and S. B. Jung: 'Effect of pin shapes on joint characteristics of friction stir spot welded AA5J32 sheet', *Mater. Trans.*, 2010, **51**, (5), 1028–1032.
100. K. Kumar and S. V. Kailas: 'The role of friction stir welding tool on material flow and weld formation', *Mater. Sci. Eng. A*, 2008, **A485**, (1–2), 367–374.
101. S. M. Chowdhury, D. L. Chen, S. D. Bhole and X. Cao: 'Tensile properties of a friction stir welded magnesium alloy: Effect of pin tool thread orientation and weld pitch', *Mater. Sci. Eng. A*, 2010, **A527**, (21–22), 6064–6075.
102. Y. H. Zhao, S. B. Lin, L. Wu and F. X. Qu: 'The influence of pin geometry on bonding and mechanical properties in friction stir weld 2014 Al alloy', *Mater. Lett.*, 2005, **59**, (23), 2948–2952.
103. P. A. Colegrove and H. R. Shercliff: '3-dimensional CFD modelling of flow round a threaded friction stir welding tool profile', *J. Mater. Process. Technol.*, 2005, **169**, (2), 320–327.
104. E. R. I. Mahmoud, M. Takahashi, T. Shibayanagi and K. Ikeuchi: 'Effect of friction stir processing tool probe on fabrication of SiC particle reinforced composite on aluminium surface', *Sci. Technol. Weld. Join.*, 2009, **14**, (5), 413–425.
105. K. Elangovan, V. Balasubramanian and M. Valliappan: 'Influences of tool pin profile and axial force on the formation of friction stir processing zone in AA6061 aluminium alloy', *Int. J. Adv. Manuf. Technol.*, 2008, **38**, (3–4), 285–295.
106. D. H. Lammlein, D. R. DeLapp, P. A. Fleming, A. M. Strauss and G. E. Cook: 'The application of shoulderless conical tools in friction stir welding: An experimental and theoretical study', *Mater. Des.*, 2009, **30**, (10), 4012–4022.
107. H. Schmidt and J. Hattel: 'A local model for the thermomechanical conditions in friction stir welding', *Model. Simul. Mater. Sci.*, 2005, **13**, (1), 77–93.
108. A. Guerra, C. Schmidt, J. C. McClure, L. E. Murr and A. C. Nunes: 'Flow patterns during friction stir welding', *Mater. Charact.*, 2002, **49**, (2), 95–101.
109. C. E. D. Rowe and W. M. Thomas: 'Advances in tooling materials for friction stir welding', Technical report, TWI, Cambridge, UK, 2005.
110. G. Buffa, J. Hua, R. Shivpuri and L. Fratini: 'Design of the friction stir welding tool using the continuum based FEM model', *Mater. Sci. Eng. A*, 2006, **A419**, (1–2), 381–388.
111. Y. Tozaki, Y. Uematsu and K. Tokaji: 'Effect of tool geometry on microstructure and static strength in friction stir spot welded aluminium alloys', *Int. J. Mach. Tools Manuf.*, 2007, **47**, 2230–2236.
112. Q. Yang, S. Mironov, Y. S. Sato and K. Okamoto: 'Material flow during friction stir spot welding', *Mater. Sci. Eng. A*, 2010, **A527**, (16–17), 4389–4398.
113. G. Buffa, G. Campanile, L. Fratini and A. Prisco: 'Friction stir welding of lap joints: Influence of process parameters on the metallurgical and mechanical properties', *Mater. Sci. Eng. A*, 2009, **A519**, (1–2), 19–26.
114. Y. H. Yin, N. Sun, T. H. North and S. S. Hu: 'Hook formation and mechanical properties in AZ31 friction stir spot welds', *J. Mater. Process. Technol.*, 2010, **210**, (14), 2062–2070.
115. Y. H. Yin, N. Sun, T. H. North and S. S. Hu: 'Influence of tool design on mechanical properties of AZ31 friction stir spot welds', *Sci. Technol. Weld. Join.*, 2010, **15**, (1), 81–86.
116. H. Badarinarayan, Y. Shi, X. Li and K. Okamoto: 'Effect of tool geometry on hook formation and static strength of friction stir spot welded aluminum 5754-O sheets', *Int. J. Mach. Tools Manuf.*, 2009, **49**, (11), 814–823.
117. Y. Tozaki, Y. Uematsu and K. Tokaji: 'A newly developed tool without probe for friction stir spot welding and its performance', *J. Mater. Process. Technol.*, 2010, **210**, (6–7), 844–851.
118. H. Atharifar, D. C. Lin and R. Kovacevic: 'Numerical and experimental investigations on the loads carried by the tool during friction stir welding', *J. Mater. Eng. Perform.*, 2009, **18**, (4), 339–350.
119. G. Mishuris and A. Plakhov: 'Magnus effect and dynamics of a spinning disc in a rarefied medium', *Arch. Mech.*, 2009, **61**, (5), 391–406.
120. C. D. Sorensen and A. L. Stahl: 'Experimental measurements of load distributions on friction stir weld pin tools', *Metall. Mater. Trans. B*, 2007, **38B**, (3), 451–459.
121. A. Arora, M. Mehta, A. De and T. DebRoy: 'Load bearing capacity of tool pin during friction stir welding', Unpublished document, The Pennsylvania State University, PA, USA, 2011.
122. R. Nandan, G. G. Roy, T. J. Lienert and T. DebRoy: 'Numerical modelling of 3D plastic flow and heat transfer during friction stir welding of stainless steel', *Sci. Technol. Weld. Join.*, 2006, **11**, 526–537.
123. R. Nandan, G. G. Roy and T. Debroy: 'Numerical simulation of three-dimensional heat transfer and plastic flow during friction stir welding', *Metall. Mater. Trans. A*, 2006, **37A**, 1247–1259.
124. R. Nandan, G. G. Roy, T. J. Lienert and T. Debroy: 'Three-dimensional heat and material flow during friction stir welding of mild steel', *Acta Mater.*, 2007, **55**, (3), 883–895.
125. R. Nandan, T. J. Lienert and T. DebRoy: 'Toward reliable calculations of heat and plastic flow during friction stir welding of Ti–6Al–4V alloy', *Int. J. Mater. Res.*, 2008, **99**, (4), 434–444.
126. M. Ota, S. Kukino, S. Uesaka and T. Fukaya: 'Development of SUMIBORON BN700 for Machining of Sintered Powder Metal Alloys and Cast Iron, SEI Technical Review, 2005, **59**, 60–65.
127. G. Grant, Y. Hovanski and M. Santella: 'Friction stir spot welding of advanced high strength steels', Oral presentation, Proc. DOE Hydrogen Program and Vehicle Technologies Program Annual Merit Review and Peer Evaluation Meeting, Arlington, VA, May 2009, DOE.
128. M. W. Cook and P. K. Bossom: 'Trends and recent developments in the material manufacture and cutting tool application of polycrystalline diamond and polycrystalline cubic boron nitride', *Int. J. Refract. Met. Hard Mater.*, 2000, **18**, (2–3), 147–152.
129. N. K. Kim, B. C. Kim, B. H. Jung, S. W. Song, K. Nakata and C. Y. Kang: 'The effect of tool geometry on the mechanical properties in a friction stir welded lap joint between an Al alloy and Zn-coated steel', *Korean J. Met. Mater.*, 2010, **48**, (6), 533–542.
130. R. Hancock: 'Friction welding of aluminum cuts energy cost by 99%', *Weld. J.*, 2004, **83**, 40.
131. Z. Feng, M. L. Santella, S. A. David, R. J. Steel, S. M. Packer, T. Pan, M. Kuo and R. S. Bhatnagar: 'Friction stir spot welding of advanced high-strength steels – a feasibility study', SAE technical paper 2005-01-1248, SAE International, Warrendale, PA, USA, 2005.
132. E. T. Turkdogan: 'Physical chemistry of high temperature technology'; 1980, London, Academic Press.
133. P. A. Colegrove and H. R. Shercliff: 'Development of Trivex friction stir welding tool Part 1 – two-dimensional flow modelling and experimental validation', *Sci. Technol. Weld. Join.*, 2004, **9**, (4), 345–351.
134. G. Padmanaban and V. Balasubramanian: 'Selection of FSW tool pin profile, shoulder diameter and material for joining AZ31B magnesium alloy – an experimental approach', *Mater. Des.*, 2009, **30**, (7), 2647–2656.
135. X. Cao and M. Jahazi: 'Effect of tool rotational speed and probe length on lap joint quality of a friction stir welded magnesium alloy', *Mater. Des.*, 2011, **32**, (1), 1–11.
136. D. Bakavos and P. B. Prangnell: 'Effect of reduced or zero pin length and anvil insulation on friction stir spot welding thin gauge 6111 automotive sheet', *Sci. Technol. Weld. Join.*, 2009, **14**, (5), 443–456.
137. P. A. Colegrove and H. R. Shercliff: 'Experimental and numerical analysis of aluminium alloy 7075-T7351 friction stir welds', *Sci. Technol. Weld. Join.*, 2003, **8**, (5), 360–368.
138. A. Scialpi, L. A. C. de Filippis and P. Cavaliere: 'Influence of shoulder geometry on microstructure and mechanical properties of friction stir welded 6082 aluminium alloy', *Mater. Des.*, 2007, **28**, (4), 1124–1129.
139. S. Gopalakrishnan and N. Murugan: 'Prediction of tensile strength of friction stir welded aluminium matrix TiC_p particulate reinforced composite', *Mater. Des.*, 2011, **32**, (1), 462–467.
140. P. Edwards and M. Ramulu: 'Identification of process parameters for friction stir welding Ti–6Al–4V', *J. Eng. Mater. Technol. (ASME)*, 2010, **132**, (3), 031006.
141. P. D. Edwards and M. Ramulu: 'Investigation of microstructure, surface and subsurface characteristics in titanium alloy friction stir welds of varied thicknesses', *Sci. Technol. Weld. Join.*, 2009, **14**, (5), 476–483.
142. P. Edwards and M. Ramulu: 'Peak temperatures during friction stir welding of Ti–6Al–4V', *Sci. Technol. Weld. Join.*, 2010, **15**, (6), 468–472.
143. H. Liu, K. Nakata, N. Yamamoto and J. Liao: 'Friction stir welding of pure titanium lap joint', *Sci. Technol. Weld. Join.*, 2010, **15**, (5), 428–432.
144. A. P. Reynolds, E. Hood and W. Tang: 'Texture in friction stir welds of Timetal 21S', *Scr. Mater.*, 2005, **52**, (6), 491–494.
145. L. Zhou, H. J. Liu, P. Liu and Q. W. Liu: 'The stir zone microstructure and its formation mechanism in Ti–6Al–4V friction stir welds', *Scr. Mater.*, 2009, **61**, (6), 596–599.

146. K. E. Knipling and R. W. Fonda: 'Texture development in the stir zone of near-alpha titanium friction stir welds', *Scr. Mater.*, 2009, **60**, (12), 1097–1100.
147. L. Cui, H. Fujii, N. Tsuji and K. Nogi: 'Friction stir welding of a high carbon steel', *Scr. Mater.*, 2007, **56**, (7), 637–640.
148. H. Fujii, L. Cui, N. Tsuji, M. Maeda, K. Nakata and K. Nogi: 'Friction stir welding of carbon steels', *Mater. Sci. Eng. A*, 2006, **A429**, (1–2), 50–57.
149. Y. D. Chung, H. Fujii, R. Ueji and K. Nogi: 'Friction stir welding of hypereutectoid steel (SK5) below eutectoid temperature', *Sci. Technol. Weld. Join.*, 2009, **14**, (3), 233–238.
150. R. Ayer, H. W. Jin, R. R. Mueller, S. Ling and S. Ford: 'Interface structure in a Fe–Ni friction stir welded joint', *Scr. Mater.*, 2005, **53**, (12), 1383–1387.
151. C. P. Cheng, H. M. Lin and J. C. Lin: 'Friction stir welding of ductile iron and low carbon steel', *Sci. Technol. Weld. Join.*, 2010, **15**, (8), 706–711.
152. Y. C. Chen and K. Nakata: 'Effect of tool geometry on microstructure and mechanical properties of friction stir lap welded magnesium alloy and steel', *Mater. Des.*, 2009, **30**, (9), 3913–3919.
153. Y. C. Chen and K. Nakata: 'Effect of surface states of steel on microstructure and mechanical properties of lap joints of magnesium alloy and steel by friction stir welding', *Sci. Technol. Weld. Join.*, 2010, **15**, (4), 293–298.
154. Y. S. Sato, A. Shiota, H. Kokawa, K. Okamoto, Q. Yang and C. Kim: 'Effect of interfacial microstructure on lap shear strength of friction stir spot weld of aluminium alloy to magnesium alloy', *Sci. Technol. Weld. Join.*, 2010, **15**, (4), 319–324.
155. M. Fazel-Najafabadi, S. F. Kashani-Bozorg and A. Zarei-Hanzaki: 'Joining of CP-Ti to 304 stainless steel using friction stir welding technique', *Mater. Des.*, 2010, **31**, (10), 4800–4807.
156. A. A. M. da Silva, E. Aldanondo, P. Alvarez, E. Arruti and A. Echeverria: 'Friction stir spot welding of AA 1050 Al alloy and hot stamped boron steel (22MnB5)', *Sci. Technol. Weld. Join.*, 2010, **15**, (8), 682–687.
157. R. Heideman, C. Johnson and S. Kou: 'Metallurgical analysis of Al/Cu friction stir spot welding', *Sci. Technol. Weld. Join.*, 2010, **15**, (7), 597–604.
158. M. Aonuma and K. Nakata: 'Effect of alloying elements on interface microstructure of Mg–Al–Zn magnesium alloys and titanium joint by friction stir welding', *Mater. Sci. Eng. B*, 2009, **B161**, (1–3), 46–49.
159. E. A. Brandes and G. B. Brook (eds.): 'Smithells metals reference book'; 1992, Oxford, Butterworth Heinemann.
160. J. F. Shackelford and W. Alexander (eds.): 'CRC materials science and engineering handbook'; Boca Raton, Florida, 2001, CRC Press.
161. J. Z. Jiang, H. Lindelov, L. Gerward, K. Stahl, J. M. Recio, P. Mori-Sanchez, S. Carlson, M. Mezouar, E. Dooryhee, A. Fitch and D. J. Frost: 'Compressibility and thermal expansion of cubic silicon nitride', *Phys. Rev. B*, 2002, **65B**, 161202.
162. A. de Pablos, M. I. Osendi and P. Miranzo: 'Effect of microstructure on the thermal conductivity of hot-pressed silicon nitride materials', *J. Am. Ceram. Soc.*, 2002, **85**, (1), 200–206.